공학석사학위논문

Machine learning-based strategy for operational intelligence of long-span bridges

머신러닝기반 장대교량 지능운영전략

2021 년 2 월

서울대학교 대학원

건설환경공학부

임 재 영

Machine learning-based strategy for operational intelligence of long-span bridges

머신러닝기반 장대교량 지능운영전략

지도교수 김 호 경

이 논문을 공학석사 학위논문으로 제출함

2021 년 2 월

서울대학교 대학원

건설환경공학부

임 재 영

임재영의 공학석사 학위논문을 인준함

2021 년 2 월

위 원 장 송 준 호 (인)

부위원장 김 호 경 (인)

위 원 조 재 열 (인)

ABSTRACT

This study proposes general development frameworks for machine-learning (ML)-based operational intelligence to assist existing bridge operational systems of long-span bridges. The frameworks address two wind-induced problems currently occurring on bridges worldwide: 1) vortex-induced vibration (VIV), and 2) accidents of vehicles overturning during typhoons.

The first part of the study introduces a developmental framework for data-driven automated VIV classification of long-span bridges. VIV is one of the most critical problems in the serviceability assessment of long-span bridges. This part proposes a structural health monitoring (SHM) data-driven framework for automated VIV classification by using a fully connected layer (FCL). VIV characteristics are analyzed using massive amounts of monitoring data of the investigated bridge, and then the appropriate features for developing the FCL are determined based on well-established wind engineering knowledge. A novel soft labeling method is suggested with pre-defined accuracy criteria for comprehensive parametric studies to build a customized classification model for each bridge.

The second part presents a developmental framework for data-driven short-term forecasting of typhoon-induced strong winds. Wind-induced accidents have become a major issue related to potential safety problems for vehicles

during typhoons. The proposed monitoring data-driven framework for short-term forecasting of typhoon-induced strong winds adopts an ML approach based on long short-term memory. The training and test data employed 17 years of monitoring data collected from both an SHM system and the Regional Specialized Meteorological Center (RSMC) in Japan. A novel grid search-based training optimization process was adopted for building a customized prediction model for each bridge. The prediction models were developed to forecast strong winds six hours in advance, which is sufficient time to prepare for the arrival of an anticipated wind disaster.

For a numerical application, the developed frameworks were applied to the Gwangan and Cheonsa Bridges, both located in South Korea, to assess their field applicabilities. The validation results provided valuable insight into how potential wind hazards could be effectively monitored using an ML-based approach to ensure the operational integrity of long-span bridges.

Keywords: Operational intelligence, Long-span bridge, Deep learning, Structural health monitoring,

Student Number: 2019-21249

TABLE OF CONTENTS

LIST OF FIGURES

LIST OF TABLES

CHAPTER 1

INTRODUCTION

1.1 Research background

Long-span bridges have always held a fascination for structural engineers because of the benefits of increased horizontal navigation clearances and reduced risks of ship collisions with piers. Nine of the ten longest bridge spans in the world have been constructed in the last 20 years (Fairclough et al., 2018). As the numbers of this type of bridge have increased, unexpected wind-induced problems have continued to occur for decades. This study investigated two major types of these problems: 1) vortex-induced vibrations (VIVs), and 2) strong wind-induced accidents of vehicles overturning.

(a)  (b) 

Figure 1-1. Two major types of wind-induced problems of long-span bridges: (a) VIVs at the 2nd Jindo bridge (2018, NAVER), (b) Accident involving a vehicle overturning on the Gwangan Bridge (2012, NAVER).

First, VIV phenomena on bridges in operation have been regularly reported globally. This is the case despite the fact that evaluations of the aerodynamic characteristics of bridge girders have been conducted and corresponding countermeasures have been greatly improved. For example, as shown in Figure 1-1(a), the 2nd Jindo bridge in South Korea experienced VIVs in 2011 due to a low damping ratio, a factor that accounted for only 70% of the design value (Seo et al., 2013). Additional wind tunnel experiments revealed that a complicated fluid-structure interaction induced by the unique configuration of the parallel bridge of this structure caused amplification of the VIV amplitude (Kim et al., 2017; Laima et al., 2013). Another example of abnormal VIV was reported by a bridge engineer who observed an abrupt VIV with significant vibration on the Yi Sun-Shin Bridge in South Korea (Hwang et al., 2020). This unusual vibration phenomenon was caused by the temporary cover over the guardrail, which changed the aerodynamic characteristics of the bridge for several hours. These phenomena indicate the difficulty of perfect VIV prediction based on wind tunnel tests alone and the possibility of abnormal vibration induced by various unexpected factors. Therefore, regular monitoring is required to achieve accurate condition assessment and sufficient serviceability during the lifetime of long-span bridges.

Second, vehicles crossing long-span bridges tend to be exposed to strong side winds. A typhoon, which usually affects coastal areas through powerful winds, has been the main reason for vehicles overturning in South Korea, as

the western North Pacific is the area most frequently hit by typhoons, six of ten of which are annually classified as Category 4 or 5 (by the Saffir-Simpson hurricane scale) (Lin et al., 2005). For example, wind-induced vehicle-overturning accidents have been regularly reported for the past decades (Baker & Reynolds, 1992; Kim & Kim, 2019; Zhu et al., 2012). Figure 1-1(b) shows two successive vehicle-overturning accidents on the Gwangan Bridge in South Korea in 2012 (Kim et al., 2020). In addition, another overturning accident occurred on a cable-stayed bridge in 2018 when a typhoon with a maximum instantaneous wind speed of over 45 m/s was passing through Japan (Al Jazeera English, 2018).

Regarding these issues, a traffic-control approach has often been adopted for most bridge operating systems. For example, bridge operators have secured driver safety by limiting vehicle speeds or restricting traffic when measured wind speeds on bridges exceeded certain thresholds (also known as critical wind speeds) (Kim et al., 2016). However, a limitation for preemptive action still exists, as at least several hours are required to implement traffic control measures after strong winds are detected. To perform these procedures effectively, accurate forecasting of typhoon-induced strong winds is essential.

1.2 Literature review

1.2.1 Vortex-induced vibration classification

The characteristics of VIVs have been successively realized and predicted in wind tunnel tests by using scaled girder section models. These are used because vortex shedding frequency is generally dominated by the shape of the structure (Bearman, 1984; Sarpkaya, 2004; Williamson & Govardhan, 2004). In addition, as the computational performance has constantly improved, computational fluid dynamics has become a practical tool to evaluate the aerodynamic characteristics of bridges (Gaarder, 2019). These methodologies are widely adopted in many design stages to develop less vulnerable girder shapes or VIV mitigation measures. Despite the effectiveness of wind tunnel tests, discrepancies between experimental results and the actual responses of a prototype bridge are inevitable. For example, a wind tunnel test is typically conducted using a two-dimensional sectional model subjected to stationary and uniform wind flows. However, experimental conditions are generally considerably more ideal than those of actual wind environments at bridge sites. Accordingly, strong turbulence and three-dimensional aerodynamic effects should be considered. In addition, unexpected structural defects in the design process can amplify experimentally obtained VIV responses. Kim et al. (2017) revealed that a

lower damping ratio than the design value could cause an excessive VIV response not observed in wind tunnel tests.

In this regard, most cable-supported bridges operate a structural health monitoring (SHM) system that can monitor static and dynamic responses in real-time. Nevertheless, the VIVs that have occurred in South Korea were first reported through citizen reports rather than an SHM system. The main reason the SHM has failed to respond proactively is that it is a classical SHM that generally sound alarms concerning structural conditions, even when monitoring data exceeds a pre-defined threshold (Ko & Ni, 2005). In other words, this approach is suitable for a preemptive response to extreme conditions such as typhoons and earthquakes but is not feasible for determining the occurrence of VIVs. For example, even when the instantaneous wind velocity reaches the critical wind velocity range, when the duration of the corresponding wind speed is not sufficient, a VIV would not be fully developed (Williamson & Govardhan, 2004). In addition, the acceleration amplitude of VIV is more often below the level of normal vehicle vibration, unlike a buffeting or flutter response.

Several studies have attempted to overcome these limitations of SHM systems by developing automated VIV classification algorithms from field monitoring data based on specific features of VIV. Huang et al. (2019) developed an automatic identification method of VIV using the random decrement technique (RDT). In their study, VIVs were classified according to a threshold for the coefficient of variation of peak values of processed data.

They assumed the ideal load conditions for buffeting and traffic loads involved a zero-mean Gaussian white-noise process. Li et al. (2017) proposed an unsupervised ML-based classification technique for VIV. The amplitude of vibration and the ratio between peaks of power spectral density (PSD) were used for feature extraction. This method was shown to be robust and practicable because it utilized the characteristics of VIVs, namely, single-mode sinusoidal vibrations with a large amplitude.

1.2.2 Short-term wind speed forecasting

Several conventional methods have been proposed over the last decades for predicting wind speed, and these can be classified into three types. The first type includes physical-based methods that utilize dynamic atmospheric models based on hydrodynamic and thermodynamic equations with specific initial and boundary conditions (Al-Deen et al., 2006; Lei et al., 2009). The second type includes statistical-based methods, including autoregressive, moving average, autoregressive moving average, and autoregressive integrated moving average models (Filik, 2016; Guoyang et al., 2005). The third type includes spatial correlation-based methods that uses the spatial relationships between measurements from different sites (Alexiadis et al., 1998; Damousis et al., 2004; Focken et al., 2002). All the aforementioned researchers have developed prediction models based on various analytical backgrounds.

Recently, with advances in information technology and computer science, studies on monitoring data-based forecasting models for the safe operations of civil infrastructures have been conducted (Bao et al., 2019). These models include: 1) traffic flow prediction (Lv, Duan et al., 2014), 2) building energy use prediction (Wang et al., 2018), and 3) wind power forecasting (Chang et al., 2015; Ding et al., 2015; Kong et al., 2017). In addition, research on short-term wind-speed prediction has utilized monitoring-data-based ML methodologies. Li and Shi (2010) conducted a comprehensive comparative study on different ML algorithms, including the adaptive linear element, backpropagation, and radial basis function, and determined that training data sources must be considered when developing prediction models. Zhang et al. (2013) and Abdalla et al. (2017) introduced hybrid artificial intelligence algorithms to improve forecasting accuracy. Wei et al. (2014, 2015, 2018) pioneered the use of ML frameworks for predicting typhoon-induced wind speeds. They showed that ML-based models could achieve more accurate results than the conventional regression and parametric wind representation methods such as the modified Rankine profile as well as the Holland and DeMaria wind profiles. For example, Wei (2014) combined an adaptive network-based fuzzy inference system with multilayer perceptron (MLP) neural networks (NNs) for use as a forecasting model and discussed the effects of typhoon tracks and intensity for a central mountain range topography. Wei (2015) introduced four kernel-based support vector machines for regression models that consisted of a radial basis function and

linear, polynomial, and Pearson VII universal kernels. Wei et al. (2018) developed a backpropagation NN model to predict highly complex nonlinear wind speeds and investigated the accuracy of wind-speed predictions at specific locations and various durations in western Taiwan.

1.3 Research objective and scope

This thesis proposes general developmental frameworks for ML-based operational intelligence of long-span bridges to improve bridge operational strategies. This research work is organized into five chapters.

Chapter 1 presents the background of this study and reviews corresponding studies (presented in chronological order) that describe preliminary methodologies for handling the two types of wind-induced problems. Literature surveys of vortex-induced vibration classification and short-term wind-speed forecasting are included in this chapter, and meaningful lessons from the investigations are discussed.

Chapters 2 and 3 describe the development of two ML-based models for automatic VIV classification and strong wind-speed prediction, respectively. These chapters examine three main areas: 1) knowledge-based feature selection, which considers the optimal combinations of influential features, 2) selection of artificial NN (ANN) models to reflect the complex relationship between environmental or vibrational characteristics and the two wind-

induced problems, and 3) performance of parametric studies on training optimization to develop a customized model for each bridge.

Chapter 4 describes the two individual developmental frameworks for dealing with the two wind-induced problems and how they are then applied to two long-span bridges to assess their field applicability. Based on the application results, the robustness and feasibility of the proposed frameworks are carefully assessed.

The final Chapter 5 provides conclusions to this research. The importance and contribution of the research are described along with prospects for future research.

CHAPTER 2

DATA-DRIVEN AUTOMATED VORTEX-INDUCED VIBRATION CLASSIFICATION

2.1 Knowledge-based feature selection

2.1.1 Vibration and wind characteristics

The Cheonsa Way Bridge is a long-span bridge linking two islands with the mainland of South Korea. It consists of one cable-stayed bridge, one suspension bridge, and multiple connection bridges. This study investigated a section of the cable-stayed bridge that includes the main span of 510 m and two side spans of 197 and 187 m, respectively. In this section of the bridge, the steel-box girder has four lanes of 18-m width supported by 108 stay cables. Two diamond-shaped concrete towers are of different heights of 195 and 135 m, respectively. The layout, dimensions, and cross-sectional shapes are shown in Figure 2-1.

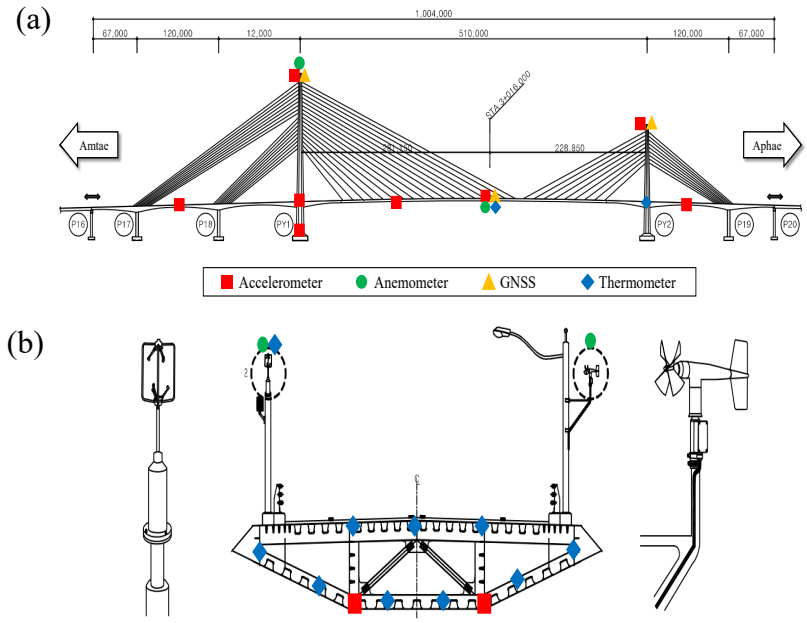

Figure 2-1. General layout (unit: m): (a) side view, (b) cross section.

A long-term monitoring dataset, collected from January to September of 2019, was used. The entire dataset was divided into 10-min segments to evaluate the vibrational and wind characteristics. Figure 2-2(a) displays the 10-min averaged wind velocity and direction collected by two anemometers. As can be seen, two strong typhoons with mean wind velocities of 47 and 37 m/s passed through the bridge in September 2019. Figure 2-2(b) shows the wind rose diagram of the 10-min averaged wind data collected by an ultrasonic anemometer, where the bold dashed line indicates the alignment of the bridge at the site. The main wind direction is shown to be mostly perpendicular to the bridge axis.

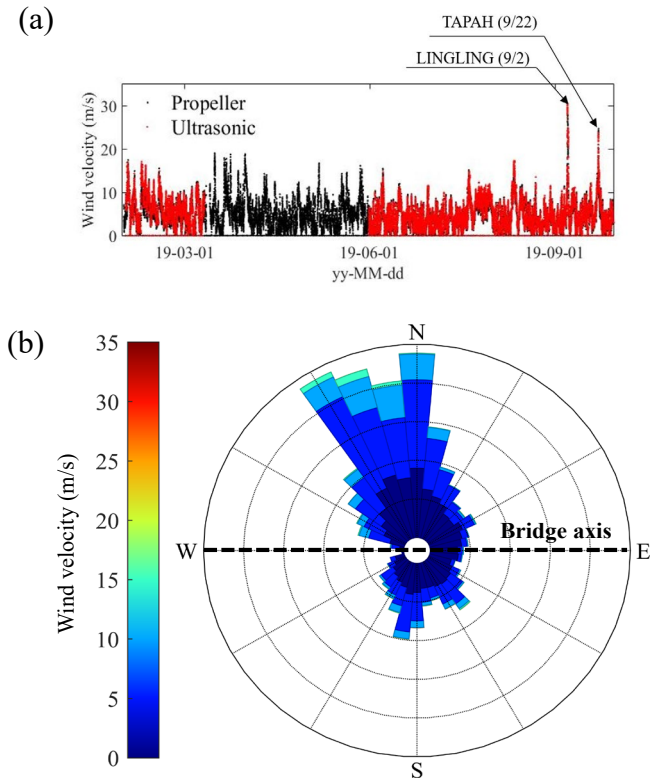

Figure 2-2. (a) 10-min averaged wind velocity, (b) wind rose diagram.

The bridge opened to the public in April 2019, and an unexpected VIV occurring for 2 h was reported in July 2019. As Figure 2-3 shows, the wind velocity ranged from 6.43 to 9.95 m/s, and the maximum acceleration exceeded the serviceability limitation of 0.5 m/s^2 (displayed as a red dotted line) as suggested by the Korean design guidelines (KSCE, 2006). Accordingly, multiple tuned mass dampers (TMDs) were installed at the mid-span in September 2019, in which four masses were elastically mounted on the vertical guide rail by six coil springs and four oil dampers.

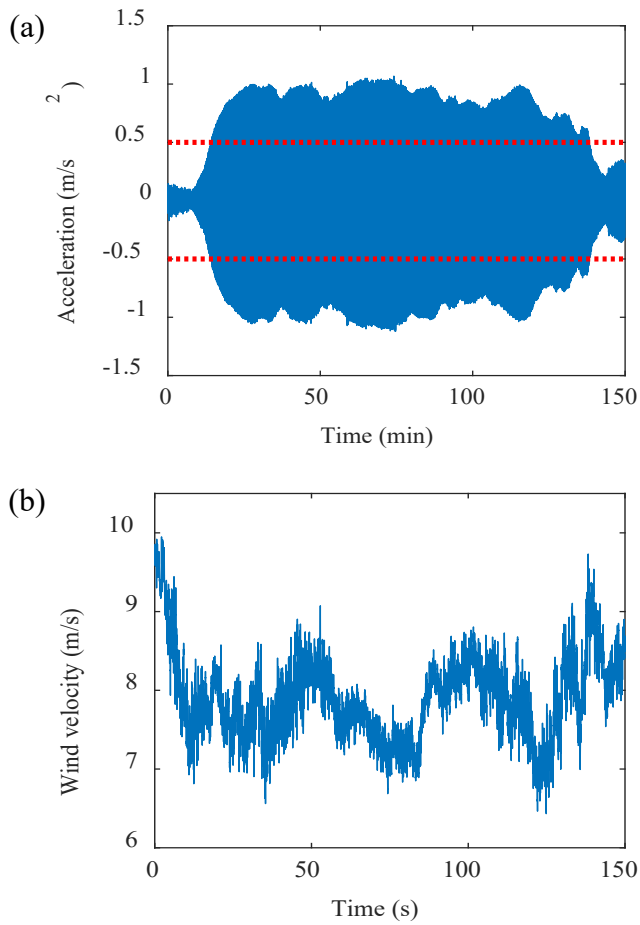

Figure 2-3. Measured VIV: (a) vertical acceleration, (b) wind velocity.

2.1.2 Feature selection

Features related to VIV phenomena should be selected to train the NN model properly (Cai, J. et al., 2018). First, the wind speed and degree should be chosen as the representative wind features because these environmental conditions have been associated with VIVs. Second, as shown in Figure 2-4, VIV induces single-mode vibrations. Therefore, the ratio between the PSD amplitude of the target and adjunct modes, defined as the PSD ratio (PR), is

typically expected to increase considerably during VIV. As a result, the four features of wind speed, wind degree, PSD amplitude of the target mode, and PR of the target mode were set as input features for training.

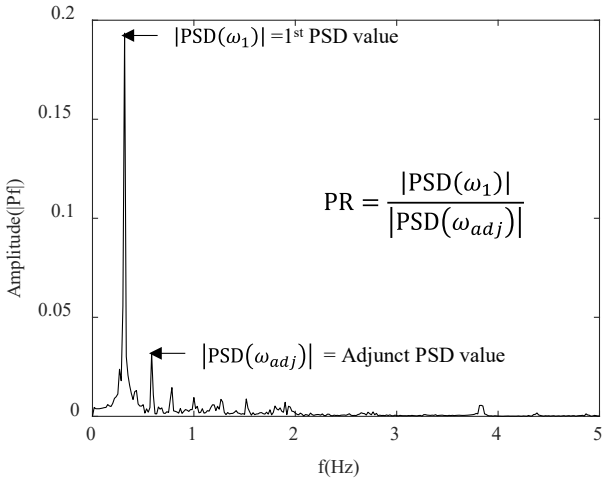

Figure 2-4. Definition of PSD ratio.

2.2 Model development

2.2.1 Literature survey: FCL

The MLP has been applied in various research fields due to its powerful and stable learning capabilities for handling nonlinear statistical data. MLP is a fully connected feedforward NN consisting of three layers: input, hidden, and output. Here, a deep neural network (DNN) involves more than one hidden layer. Many studies have demonstrated that DNNs have achieved significant performance in extracting the complex relationships between inputs and outputs in massive data by updating the weights of each neuron

connection and bias using a backpropagation algorithm (Cai et al., 2018). This capability enables learning complex nonlinear representations between occurrences of VIVs and corresponding environmental conditions

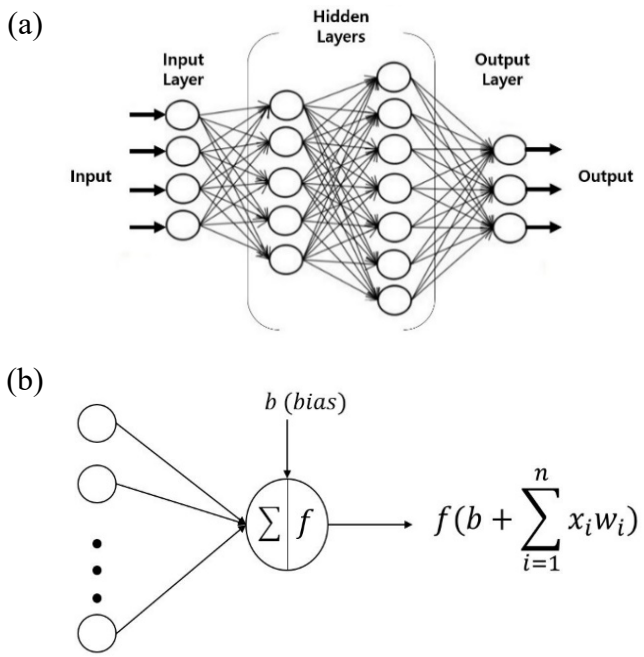

Figure 2-5. (a) MLP, (b) pathway signal flow calculation.

Figure 2-5(a) shows one example of an MLP having two hidden layers with four input and three output nodes. When input data are given to this NN, each neuron computes the output using the specified activation function (depicted by a circle in Figure 2-5(b)). The basic formula is given by

$$v_j = G_j\left(b + \sum_{i=1}^{n} x_i w_i\right) \tag{1}$$

where v_j is the output of each neuron, w and b are the weight and bias to be trained, respectively (in which n is the number of inputs), and $G_j(\cdot)$ is the activation function of the j-*th* neurons in the current layer. The following three functions are commonly used for G_j: 1) rectified linear units (ReLUs), 2) tanh, and 3) sigmoid. After the final values are obtained through the hidden and output layers that process the input data and send it up to the next layer, the total error is calculated using the following equations.

$$E_k = \frac{1}{n_o}\sum_{i=1}^{n_o}|v_i - t_i| \tag{2}$$

$$\boldsymbol{E}(\boldsymbol{w},\ \boldsymbol{b}) = \frac{1}{N}\sum_{k=1}^{N} E_k \tag{3}$$

In (2), v_i and t_i are the calculated and actual values of the i-th neuron, respectively, where n_o denotes the number of neurons in the output layer. In addition, E_k is the error of the k-th data. The relationship between the averaged error $\boldsymbol{E}$ and trainable variables $(\boldsymbol{w}, \boldsymbol{b})$ is described by (3). The main objective of the training was to minimize the total error, where the error gradient for each neuron in the hidden layer was iteratively computed while the weights and biases were updated.

2.2.2 Model design

The FCL was selected as the basic structure of the developed NN model. The network uses wind and vibrational features as the input values and consists of several hidden layers. An ReLU was used as the activation function for all hidden layers. Sigmoid was applied at the end of the NN for binary classification purposes, where the output values represent the probability that a given sample will be classified into the VIV class.

A binary cross-entropy was selected to estimate the loss function to update the network using gradient descent following each training epoch. To train the NN effectively and to prevent the overfitting problem and improve the robustness of the model, weight decay and L2 regularization (Krogh & Jertz, 1992) and Dropout (Srivastava et al., 2014) were previously adopted. The NN weights were initialized by Glorot normalization and then updated by an Adam optimizer (Kingma & Ba, 2014), where all processes were executed using Python and Google TensorFlow (Abadi et al., 2016). The detailed parameters are shown in Table 2-1 and Figure 2-6.

Table 2-1. Model design parameters

Parameter	Setting Value	Remarks
Dimension of input data	4	Four selected features
NN structure	FCL Dropout	Each layer has 40 nodes Dropout ratio = 20%
Activation function	ReLU sigmoid (end node)	L2 regularization weight decay = 0.001
Ratio between train, val, and test	70:20:10	-
Loss function	Adam	Learning rate = 0.001
Training optimizer	Binary cross-entropy	Binary classification
Training epochs	50	-
Batch size	100	-

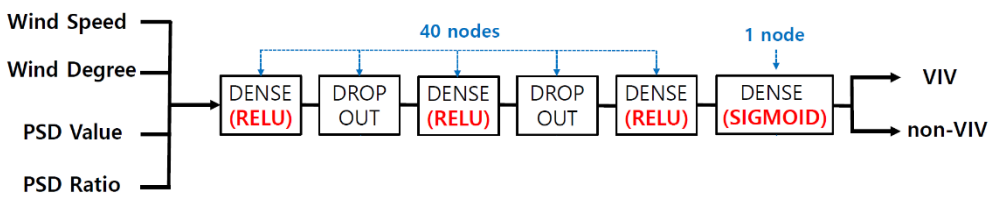

Figure 2-6. NN model structure for VIV identification.

When training begins, negative and positive datasets are randomly selected from each labeled dataset, where the proportion of the two groups is maintained at a value of 1. Then, the network parameters of the model are updated based on the error gradients derived from the loss function in each epoch. When the validation loss does not significantly decrease for five epochs, the training process is automatically terminated and optimal parameters of the NN are chosen again.

2.3 Training optimization

2.3.1 Soft labeling method

Data labeling is one of the essential processes in supervised learning applications. With respect to VIV, the distinction between VIV and non-VIV is ambiguous, which means that the classification performance could be poorer due to heuristic errors during the labeling process. For example, Figure 2-7 shows the relationship between the 1-min peak factor and corresponding 1-min averaged wind velocity. This graphically demonstrates the significance of the peak factor in the case with different sources of vibration. The peak factor of vertical acceleration was reduced by as much as 1.5 in the wind speed range of 5 to 12 m/s when VIV was observed, whereas it was much lower than that under normal operation or high wind velocity. Although VIVs with a peak factor close to 1.5 could be easily identified, clearly distinguishing between VIV and non-VIV cases in the higher range of peak factors such as 1.5 to 2.5 was not easy. Another problem was that the amount of monitored data was generally too large, thus inspecting inspect each raw data to label every VIV and non-VIV could be a time-consuming process. To handle these difficulties, this study introduced a soft labeling method, which is a simple data labeling approach that applies specific threshold values to divide monitored data into two classes. The peak factor was selected as the

threshold to label each sample to VIV and non-VIV cases, and this threshold is called a peak factor threshold (PFT).

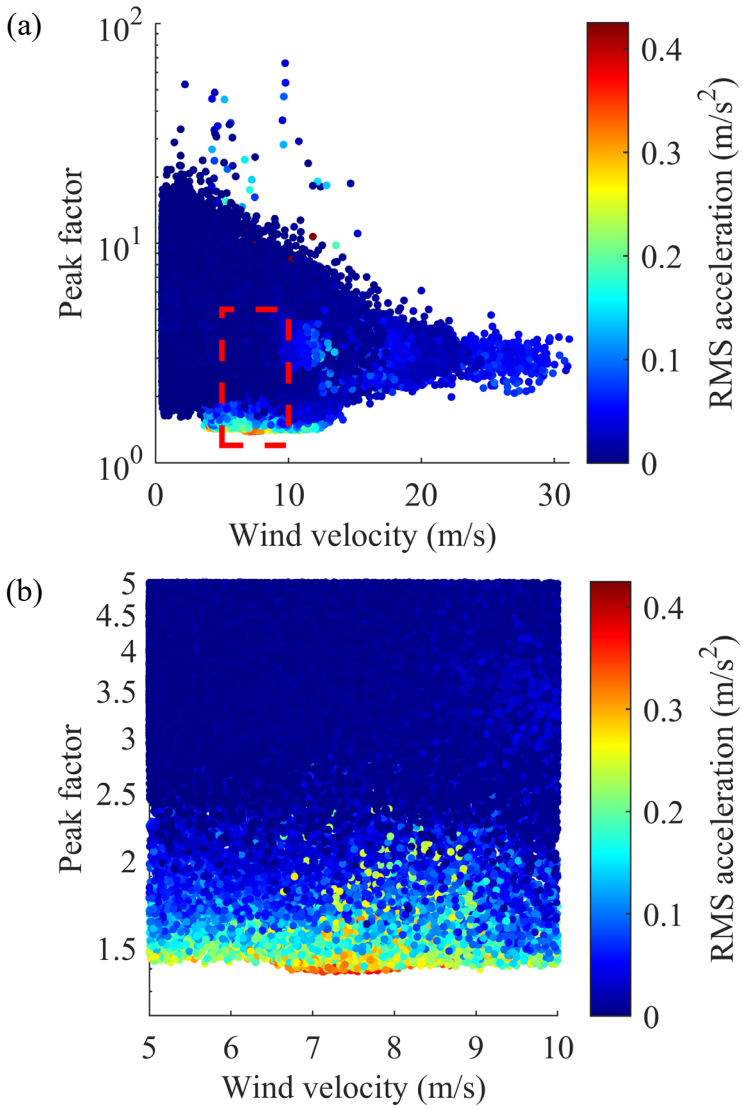

Figure 2-7. (a) Peak factor of vertical acceleration according to wind velocity, (b) zoomed.

As Figure 2-7 shows, the peak factor of measured acceleration gradually decreased as the bridge was subjected to VIV. It then approximated 1.5 when

VIV was entirely governed. A PFT of 1.5 results in strict labeling regarding all weak VIV as non-VIV cases. However, a PFT of 2.5 can lead to imprecise labeling by including too many non-VIV as possible cases. Therefore, a certain degree of mixture of VIV and non-VIV in both labeled classes is inevitable, which means that setting the PFT value for the labeling process can be complicated. Therefore, a comprehensive parametric sensitivity analysis should be performed to find an optimal PFT range.

2.3.2 Semi-VIV class

Figure 2-8 gives the definition of CMA for four areas of binary classification results, namely, true positive (TP), true negative (TN), false positive (FP), and false negative (FN) predictions.

Predicted label \ Actual label	1 (VIV)	0 (non-VIV)
1 (VIV)	**TP (true positive)** • Correct Prediction • Predict VIV as VIV	**FP (false positive)** • Type I error • Predict non-VIV as VIV
0 (non-VIV)	**FN (false negative)** • Type II error • Predict VIV as non-VIV	**TN (true negative)** • Correct rejection • Predict non-VIV as non-VIV

Figure 2-8. Confusion matrix for binary classification.

Of these, the samples in the FP class can be interpreted as follows: samples could be classified into the VIV class even though they were initially classified as non-VIV by the soft labeling method due to their higher peak

factor as compared with the PFT. In computer science, these FP classes are often undesirable because they lower the precision of the training model. The soft labeling approach was thus introduced to divide weakly the monitoring data based on the PFT and allow the NN model to classify test data precisely into VIV and non-VIV classes based on the trained wind and vibrational characteristics. Therefore, the FP samples can be re-interpreted as follows: weak VIV also having similar wind and vibrational characteristics as those of VIV with a peak factor higher than the PFT (referred to as a "semi-VIV" case), which includes the cases in the developing stage of VIV or along with other types of bridge excitation such as traffic loads.

2.3.3 Parametric studies on PFT for model tuning

A comprehensive parametric study on PFTs was conducted to find the optimal PFT range. Figure 2-9 shows histograms of the peak factors collected for the considered period. The distributions concentrated around a peak factor of 3.0. However, another local maximum also could be found in the peak factor range of 1.5 to 1.7, which was due to the VIVs. This implies that the peak factor distribution for VIVs is in the range of 1.5 to 1.7, which is different from that of the normal operation. In other words, if the peak factor of the classified VIV cases concentrated to 3.0 rather than 1.5–1.7, it means that the developed network has no VIV classification capabilities at all. When FP includes only semi-VIV cases, the distribution of peak factors of the FP

class would be skewed to the left side and apart from that of the total dataset. However, as FP contains misclassified non-VIV cases, the peak factor distribution of the FP should gradually resemble the overall distribution. In this study, the Bhattacharyya distance (BD), which measures the similarity of two probability distributions, was employed to quantify the similarity between these two types of distributions, that is, the peak factor of positively classified cases and the whole dataset. This enables us to evaluate how well the model can distinguish VIVs among mixed vibrations according to different PFT settings.

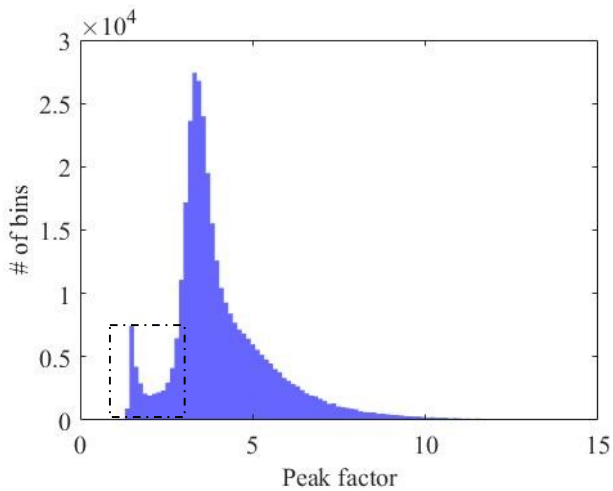

Figure 2-9. Histogram of peak factor during the monitoring period.

Table 2-2 shows comparisons of the positively labeled numbers. Figure 2-10(a) and 11(a) show the total FP counts and corresponding peak factor distributions according to the different PFTs, respectively. The distributions of positively predicted samples, which were previously defined as TP and FP, and the total dataset are plotted in blue, red, and gray bars, respectively.

In general, the use of imbalanced datasets unavoidably requires sufficient positive cases to train the model on the selected features. If a small number of positive samples is employed, such as a peak factor below 1.7, the developed model would underfit the training data. The NN, subjected to underfitting, cannot detect positive cases specifically. This results in increased FP counts. However, despite the increased number of FPs, the positively classified distributions are skewed mainly toward the left in contrast to the histograms of the natural peak factor. In addition, the distributions of FP are found to be totally different from that of the total dataset when PFT is set to a low value. This is supported by Figure 2-10(b), which illustrates Bhattacharyya distance (BD), clearly showing the decline in the degree of discrepancy between the distribution of positively classified data sets and that of the total dataset as PFT increased. When the PFT was between 1.5 and 1.9, the BD was relatively high, which means that the peak factor distribution of FP had completely different properties from that of the total data. This result agreed with the hypothesis that the trained model with a soft labeling method could classify the semi-VIVs into FP classes. By contrast, as the PFT exceeded 2.0, the distribution of FP gradually began to resemble the distribution of the total data. The higher PFT included the non-VIV cases as positively labeled samples, which gradually diverged from the ideal VIV specific classification. Accordingly, the training process intrinsically involved a greater number of opportunities to learn unrelated features from the training datasets. This resulted in the FP counts dramatically increasing and the

positively predicted distribution to be similar to the histograms of the natural peak factor shown in Figure 2-9.

Table 2-2. Positive labeled datasets

PFT	Num. of datasets	Num. of positive datasets	Percentage (%)
1.5	346999	5309	1.5
1.6		9858	2.8
1.7		12847	3.7
1.8		15076	4.3
1.9		16763	4.8
2.0		18249	5.3
2.5		29709	7.7
3.0		81952	14.9
3.6		332730	46.9

(a)

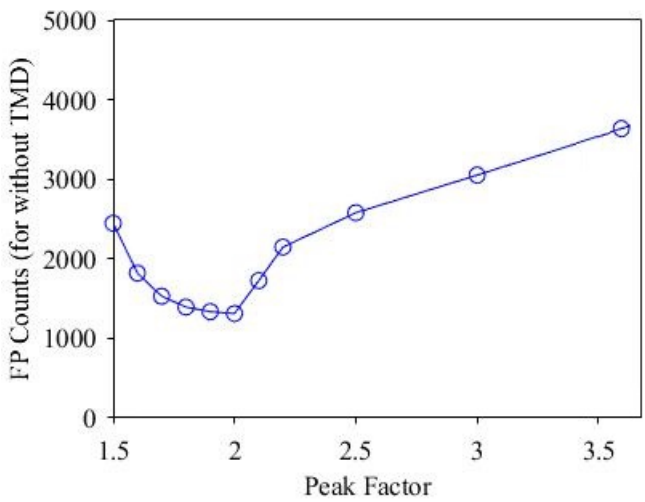

(b)

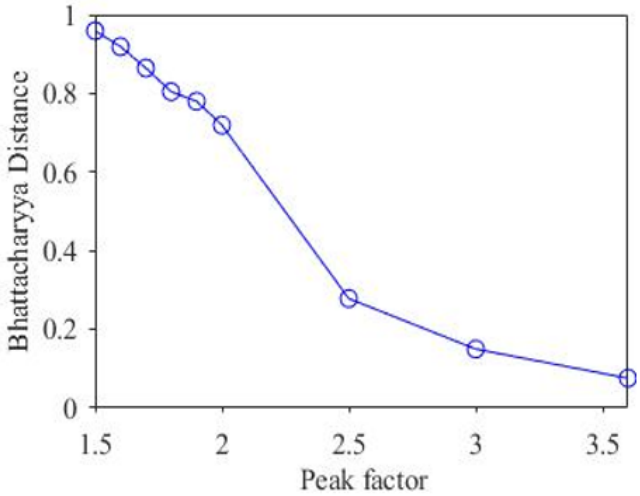

Figure 2-10. (a) FP counts, (b) Bhattacharyya distance according to different PFTs.

The trends of the velocity-acceleration (VA) curve shown in Figure 2-11(b) agreed well with these trends of accuracy criteria. Here, red, blue, green, and black dots represent TP, FP, TN, and FN, respectively. When the PFT was 1.5, most semi-VIV samples could be classified as non-VIV because of excessively strict labeling conditions, and accordingly, the VA distribution of the FP class nearly overlapped with that of the TP. As the PFT increased gradually, the area of FP decreased. At 1.7, the TP, FP, and TN properly represented the areas of fully developed VIV, semi-VIV, and non-VIV, respectively. This trend continued until the PFT reached 2.0. However, afterward, most of the semi-VIV cases were classified into TP, and FN cases sharply increased. Therefore, considering these tendencies in the accuracy criteria, the optimal PFT range could be considered to be 1.5 to 2.0.

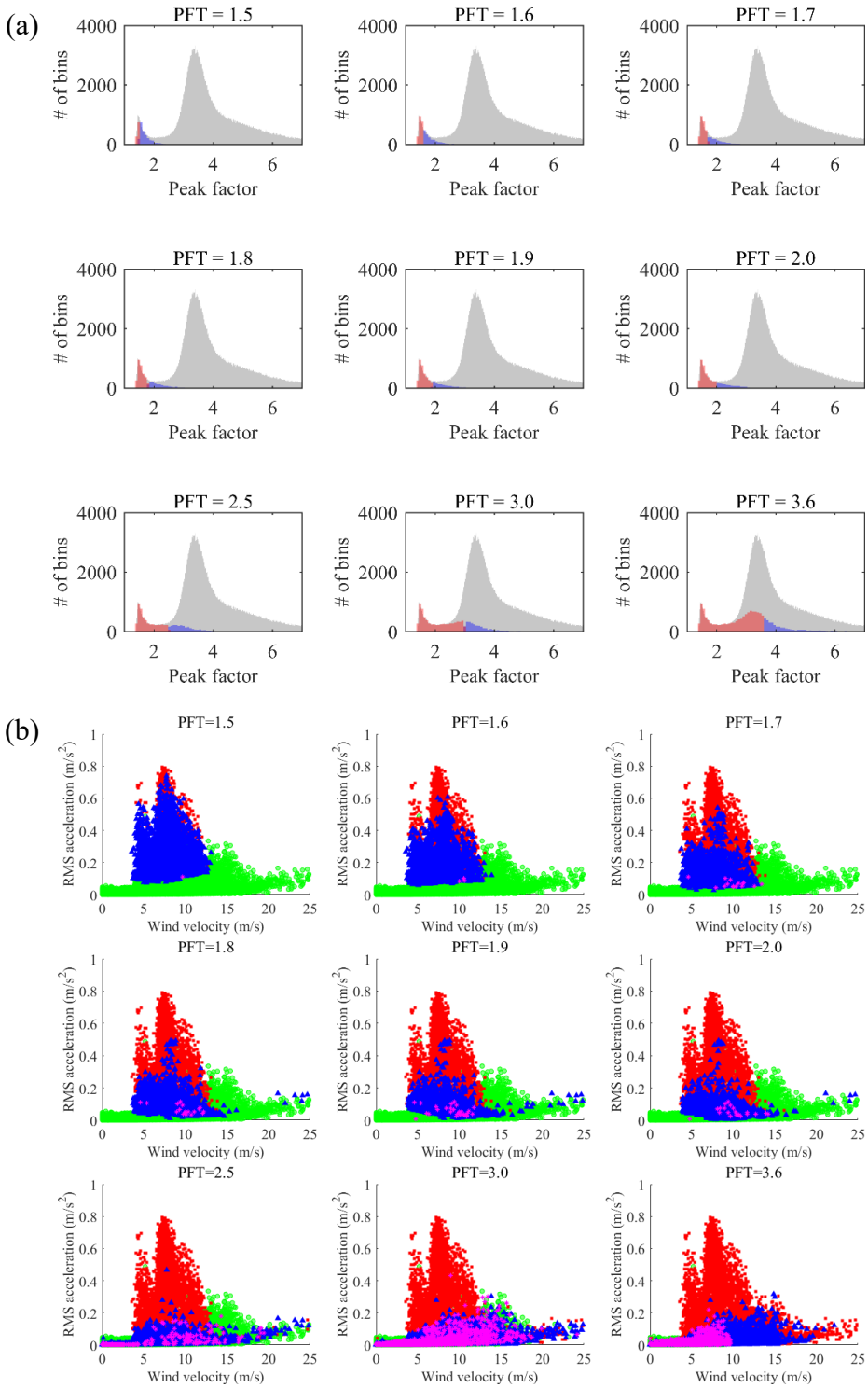

Figure 2-11. Classification results according to PFTs: (a) positively predicted distribution, (b) VA curve.

CHAPTER 3

DATA-DRIVEN SHORT-TERM FORECASTING OF TYPHOON-INDUCED STRONG WINDS

3.1 Knowledge-based feature selection

3.1.1 Typhoon-induced strong wind characteristics

The Gwangan Way Bridge (GWB), which is located in the southeastern part of South Korea, as shown in Figure 3-1(a), is an ocean-side double-deck suspension bridge. It consists of a cable-stayed bridge and two connection bridges. For all bridge sections, the total length of the bridge is 7.4 km, and the traffic lanes on the upper and lower decks are south- and northbound, respectively. The layout and dimensions are shown in Figure 3-1(b). The bridge opened to the public in January 2003, and two consecutive and entirely unexpected accidents involving vehicles overturning occurred on the bridge in 2012 during a typhoon. Kim et al. (2020) found that those accidents were mainly due to a large increment in wind-speed acceleration between the upper and lower decks. This is the so-called wind tunneling effect and means that vehicles traversing this type of bridge are more vulnerable to strong winds during a typhoon. Two types of monitoring data sources were used for this study: 1) structural health monitoring (SHM) data, and 2) data from the Regional Specialized Meteorological Center (RSMC). First, SHM systems

are typically operated at the beginning of a bridge's construction to check current environmental conditions in real-time. For the GWB, wind anemometers (RM-Young 05106) were installed on the cable-stayed bridge at the top of the pylon for real-time monitoring purposes, as illustrated in Figure 3-1(b). The wind data, consisting of speed and direction, were collected at a sampling frequency of 100 Hz.

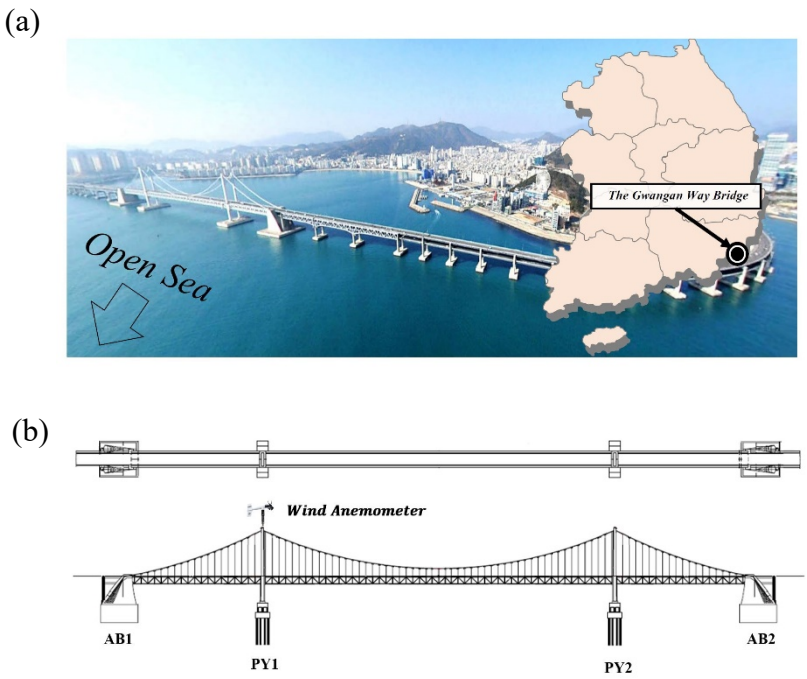

Figure 3-1. Gwangan Way Bridge: (a) location, (b) side view.

Second, typhoon information obtained from the RSMC database was collected over a six-hour period by sensors onboard the orbiter, and consisted of the physical properties of a typhoon, including latitude, longitude, central pressure, maximum sustained wind speed (MSWS), and radius. Figure 3-2

shows typhoon routes from 2003 to 2019 in the western North Pacific and the South China Sea. More than 400 typhoon events occurred during this period. They generally developed on the side of the subtropical ridge closer to the equator, and then some of them moved poleward past the ridge axis before recurving north and northeast, affecting South Korea and Japan (Center, 2007; Landsea, 2014).

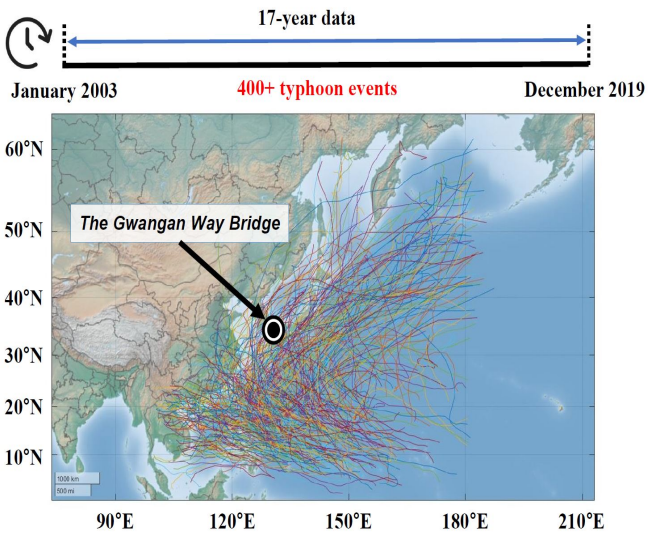

Figure 3-2. Typhoon routes obtained from RSMC database.

These two types of data sources were collected for 17 years from 2003 to 2019. To transform the separated original data into a combined form, all collected data were preprocessed to be evenly spaced at one-hour intervals and then merged, as shown in Figure 3-3.

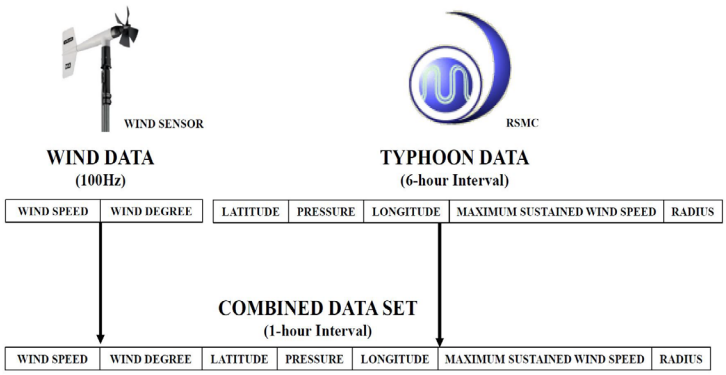

Figure 3-3. Combined monitoring data set.

3.1.2 Feature selection

Because a vehicle's vulnerability is greatly influenced by strong wind speed at a bridge, careful investigations on the influential parameters of this type of hazard during a typhoon can be critical for improving prediction performance. According to previous studies, the maximum sustained wind, which generally occurs at an inner radius of a typhoon's eyewall and where the air begins to ascend to the top of the troposphere and has the strongest near-surface winds, can be a good indicator of the intensity of a typhoon (Blanchard & Hu, 2005). Three past typhoon cases were examined to explore the relations between the physical properties of a typhoon and strong winds at a bridge. The physical properties included the distance between the bridge and typhoon center, pressure, and MSWS. Figure 3-4 illustrates the time histories of selected features with corresponding measured wind speed at the bridge, clearly demonstrating that strong wind speeds tend to occur after the distance and

pressure are at their lowest points, with the maximum share of wind power (MSWP) at its highest point. This study assumed that a sequence-based NN model could be trained on these specific trends of the selected features.

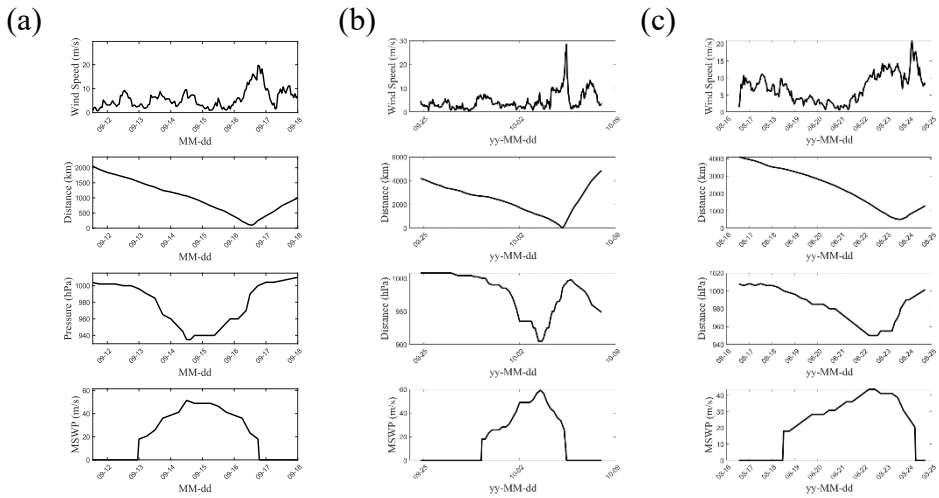

Figure 3-4. Time histories of selected features and corresponding wind speeds at the bridge: (a) NARI (09/2007), (b) CHABA (09/2016), (c) CIMARON (09/2019).

3.2 Model development

3.2.1 Literature survey: Long Short-Term Memory

A recurrent NN (RNN) is an ANN model used to solve sequence-based problems. A fundamental difference exists between MLP and RNN. Unlike the MLP, whose structure allows signals to travel one way from input to output, the RNN has other connections to form a directed graph along a temporal sequence, enabling those connections to exhibit temporal dynamic

behavior and use their internal state memory to process variable-length sequences. The RNN can be converted into multilayer feedforward networks, where a new layer is subsequently added at each time step. Due to its circular flow, computational results from the previous time step can be fed back into the model. These feedback networks are dynamic and their internal states change continuously during processing (Dupond, 2019). The basic formula is given as follows and shown in Figure 3-5.

$$h^{(t)} = f\left(h^{(t-1)}, x^{(t)};\ \theta\right) \tag{4}$$

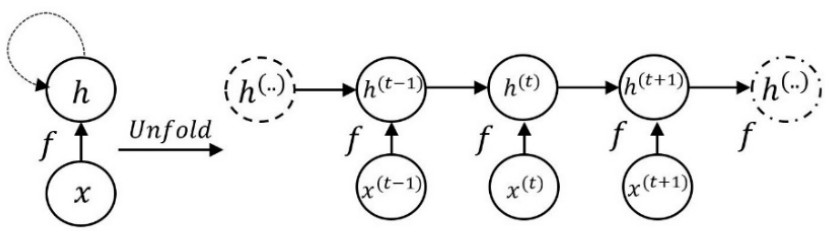

Figure 3-5. Folded and unfolded recurrent layers.

where $h^{(t)}$ is the current hidden state of the model and a function f of the previous hidden state h(t-1), current input data x(t), and parameters θ.

The long-short-term memory (LSTM) introduces new features called gated cells to the original RNN (Hochreiter & Schmidhuber, 1997). Three types of gates are used, namely, input, output, and forget, as shown in Figure 3-6, and this additional control system enables LSTM to regulate the flow of

signals into and out of the model for storing critical information that has accumulated over time.

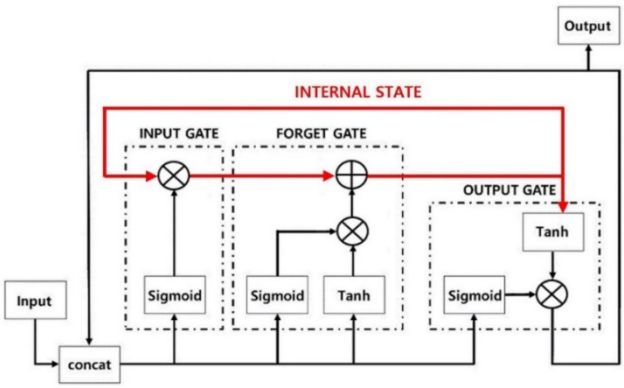

Figure 3-6. LSTM model.

3.2.2 Model design

The LSTM layer is selected as the basic structure of the developed NN model. Based on the identified strong wind characteristics, the developed model uses wind speed at the top of the pylon, maximum sustained wind, pressure, speed, and distance between a typhoon and the bridge as training features. It consists of three LSTM layers. A mean absolute error (MAE) is selected to estimate a loss function to update the network using gradient descent after each training epoch. Then, the NNs are updated using an RMSprop optimizer 61, where all the processes are executed using Python and Google TensorFlow (Abadi et al., 2016). The detailed parameters are shown in Table 3-1 and Figure 3-7.

Table 3-1. Model design parameters

Parameter	Setting Value	Remarks
Time unit	1 h	-
Length of input data	10 h	-
Length of output data	1 h	-
Prediction interval	6 h	-
NN structure	3-layered LSTM	30 nodes
Ratio between train and val sets	7:3	-
Loss function	MAE	-
Training optimizer	RMSprop	-
Training epochs	50	-
Batch size	100	-
Number of generated model	30	For each training case

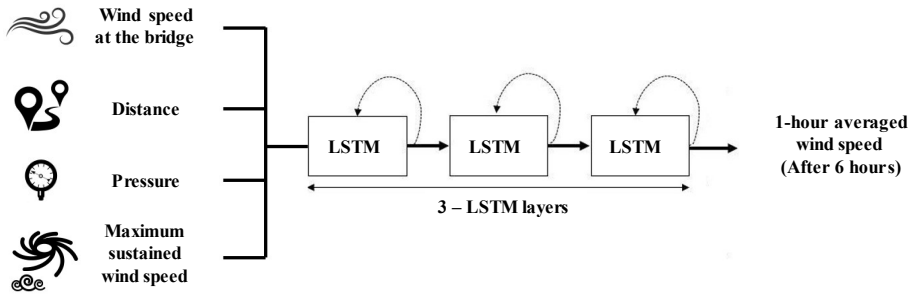

Figure 3-7. NN model structure for strong-wind prediction.

3.3 Training optimization

3.3.1 Typhoon routes

Considering the paths of typhoons that typically sweep across the Korean peninsula, two representative approach routes can be used based on the GWB location, namely, sea and inland routes, as graphically illustrated in Figure 3-8. In this case, typhoon routes can be classified automatically using k-means clustering with two pre-defined features and a reference angle.

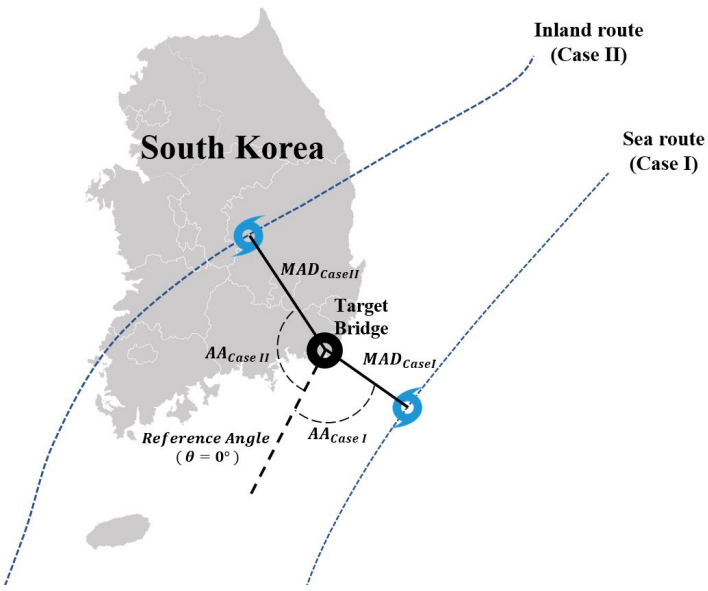

Figure 3-8. Selected features of the K-means clustering.

K-means clustering is a useful algorithm that aims to divide n observations into k sub-clusters in which each observation belongs to the cluster with the closest mean value (MacQueen, 1967). The clustering mechanism proceeds

by selecting k initial cluster centers and then iteratively refining them. This process continues until no additional variation occurs in the assignment of data points to clusters in the previous step. The basic formula used is given by the following equations.

$$d(x,y)^2 = \sum_{j=1}^{M}(x_j - y_j)^2 = \|x-y\|_2^2 \tag{6}$$

$$SSE = \sum_{i=1}^{n}\sum_{j=1}^{k} w^{(i,j)}\left\|x^{(i)} - \mu^{(j)}\right\|_2^2 \tag{7}$$

In (6), the index j denotes the j-th dimension of the variable x and y, and $d(x,y)^2$ is the square Euclidean distance between the two points. In (7), $\mu^{(j)}$ is the representative points and $w^{(i,j)}$ is the binary variable. If the data point is assigned to cluster j, $w^{(i,j)}$ is 1, otherwise 0. The k-means algorithm itself is an optimization problem for identifying the optimal clustering centers by minimizing the sum of squared errors. The first feature is the minimum approach distance (MAD) between a typhoon and the bridge. The second is the approach angle (AA) between a typhoon and the bridge when a typhoon is in MAD. The AA measures an angle such that 0 degrees starts from the reference angle and increases in a clockwise direction. The reference angle value is chosen to ensure that all typhoons passing through the Korean peninsula are appropriately classified into two separate categories. Prior to clustering analysis, feature scaling was used to normalize the original data by the min-max method (Han. et al., 2011). Figure 3-9 shows scatter plots for

the original and normalized scales. Figure 3-10 illustrates the clustered results categorized into sea and inland routes as well-intended.

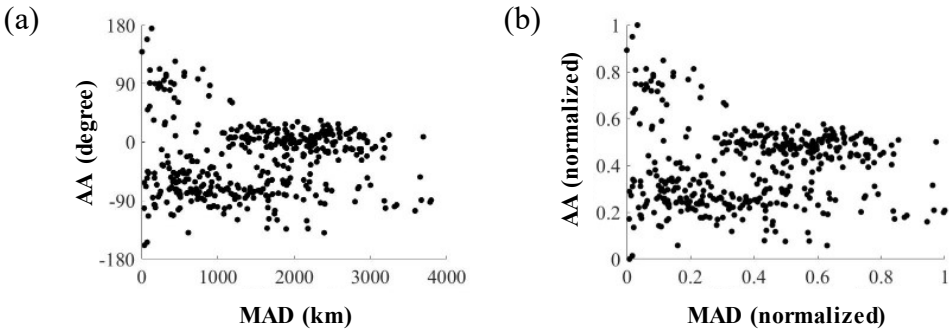

Figure 3-9. Scatter plots for the selected features: (a) original, (b) normalized.

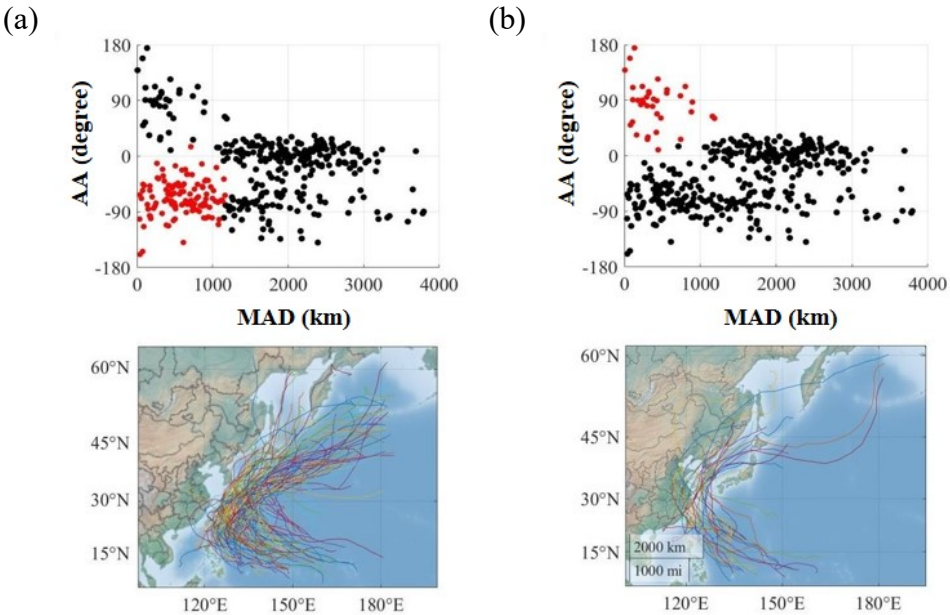

Figure 3-10. Clustered typhoon routes (red dots): (a) sea route, (b) in-land route.

3.3.2 Influential typhoon

Some of the typhoons that have swept across the Korean Peninsula did not increase the wind speed at the bridge to one deemed critical. The training process should be based on influential typhoon cases to build a strong wind-specific prediction model. Therefore, the minimum wind speed requirement in this study was set by referring to previous studies when training datasets were selected. Baker & Reynolds (1992) suggested that traffic movement should be restricted when instantaneous wind speed is greater than 20 m/s for all vehicles, where the threshold is the expected maximum 3-s gust velocity that will occur during the hour of an accident. However, differences exist in terms of averaging periods and altitudes between wind speed as suggested by Baker & Reynolds (1992) and the one used in this study. Therefore, a direct comparison between the two values is not reasonable. Thus, altitude adjustment between the two types of wind speeds is required to utilize the conversion factor, as the guideline is based on an elevation of 10 m above sea level. It is assumed that the mean near-surface wind speed under strong wind conditions, which is typical of typhoons, can be estimated using an equilibrium form of the logarithmic boundary layer profile as described by the following equation (Lumley & Panofsky, 1964; Powell. et al., 2003).

$$V(z) = \frac{u_*}{k} \ln\left(\frac{z}{z_0}\right) \tag{8}$$

where $V(z)$ is the converted wind speed at height z, z_0 is the representative surface roughness length (z_0), k is von Karman's constant (assumed to be 0.41), and u_* is the friction velocity.

Converting the instantaneous wind speed to a 1-h averaged value by using guidelines for converting between various wind averaging periods in typhoon conditions has been previously suggested (Harper. et al., 2010). Several different location categories and additional sub-categories were assigned based on the GWB location. Because the bridge is located close to the coastal area, the "off-sea" class was selected as the sub-category. Table 3-2 summarizes the selected parameters for converting between wind speeds of different wind averaging periods.

Table 3-2. Selected parameters for converting wind speeds

	Terrain type	**Gust duration(s)**	**Reference period (s)**	**Surface roughness length(z_0)**
Setting	Off-Sea	3	3600	0.005

Finally, the threshold wind speed at the top of the pylon was estimated to be 15 m/s, and the data sets satisfying the above condition were selected for the model training. As a result, a total of 26 typhoon events were found, where 13 of them belong to East Sea Route, and the rest belongs to the Inland Route, as illustrated in Figure 3-11.

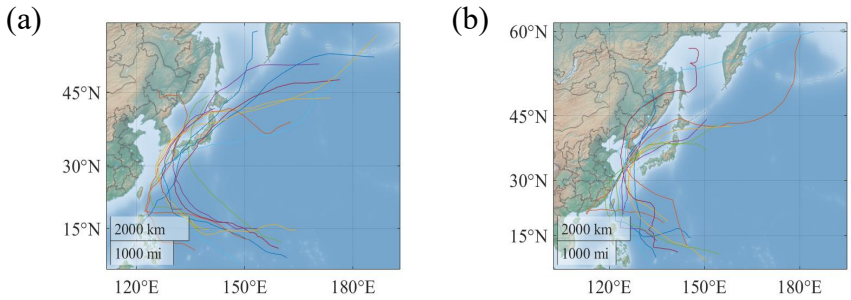

Figure 3-11. Influential typhoon routes: (a) East Sea route, (b) inland route.

3.3.3 Time-delay analysis for past typhoons

Because of the different climatological effects on wind speeds at different bridge locations, the relation between the time histories of selected features and strong wind speeds should be carefully examined to build a customized prediction model. Figure 3-12(a) shows a 3D scatter plot for three-time delay criteria, where DD, PD, and MSWPD denote the distance delay, pressure delay, and maximum sustained wind speed delay, respectively. For example, as shown in Figure 3-4, the definition of DD is the time difference between the minimum point of distance and maximum point of wind speed at the bridge. The others are defined based on the same principle, except for the MSWPD case, which considers the maximum instead of the minimum point.

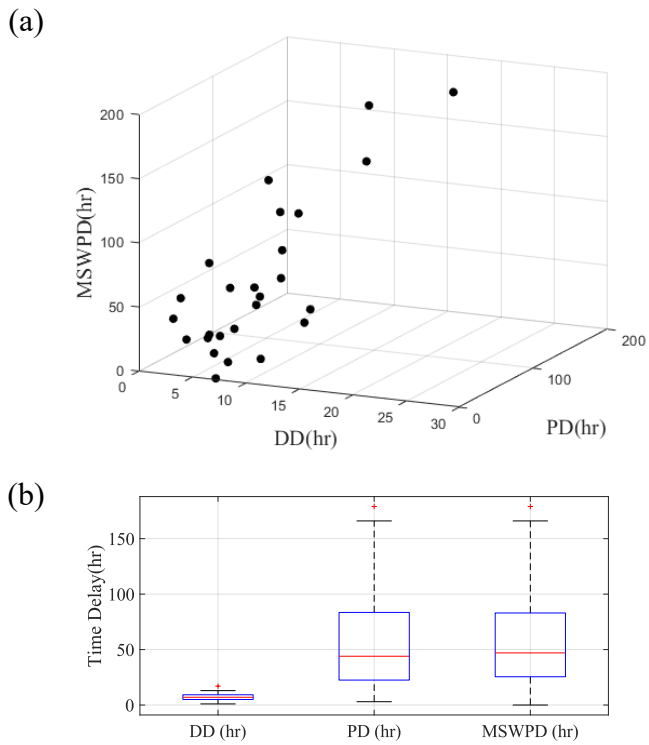

Figure 3-12. Time-delay analysis: (a) 3D scatter plot, (b) box-plot distribution.

Interestingly, there are distribution discrepancies between each indicator. For example, Figure 3-12(b) illustrates a box-plot distribution showing that the maximum wind speed tends to occur at approximately a mean value of 7 h after the minimum point of distance, whereas the pressure and MSWS are approximately 50 h on average. This gives us useful information about how to design a typhoon-induced strong-wind prediction model. To reflect carefully the natural time discrepancies of delay distributions, new parameters called second starting point (SSP) and history duration (HD) were additionally defined. These are necessary to perform manual corrections by

applying additional time delays to the pressure and MSWS features when generating training datasets, as shown in Figure 3-13

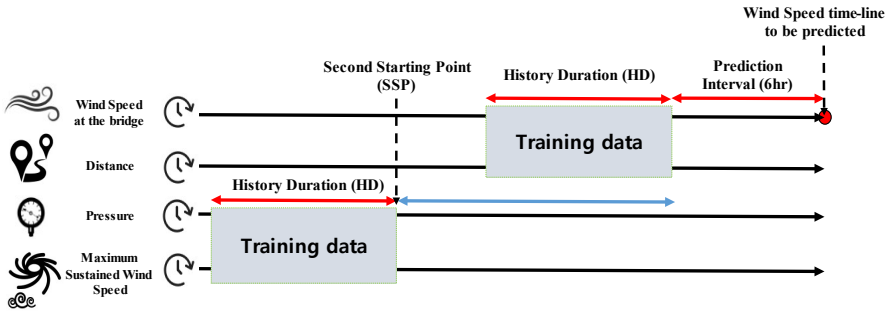

Figure 3-13. Definitions of SSP and HD.

3.3.4 Grid search-based model tuning

Numerous combinations can be generated for the selection of values of HD and SSP. In this study, a grid search method was used that involved scanning the two parameters to identify automatically the optimal one resulting in the most accurate prediction. In the appendix, the influential typhoons are listed in Table A.1-1. Of those listed, the typhoon MITAG was selected for the model tuning process, and its detailed information is presented in Figure 3-14. If the proposed prediction model were well-tuned during this process, the occurrence time of strong wind speed of the tuning dataset could be predicted with accuracy.

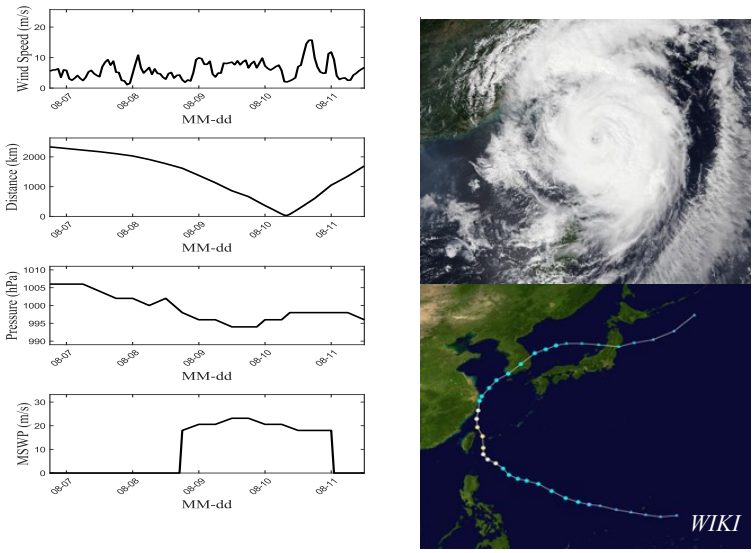

Figure 3-14. Detailed information of tuning data: MITAG (09/2019).

The performance of the NN model varies depending on the initialization of the weights and randomly split training and validation partitions. For this reason, an optimization objective function generally tends not to converge to a global minimum but instead to a local one because numerous methods can be employed to train it (Wu et al., 2013). To check the stability of the prediction results, each training process was repeated 30 times to calculate the mean and standard deviation of the MAE.

Figure 3-15 shows grid search results, where the z-axis value on each grid is an average MAE value for 6 h before and after the actual maximum wind speed. This clearly demonstrates that low MAE values were found in a certain range of the selected parameters.

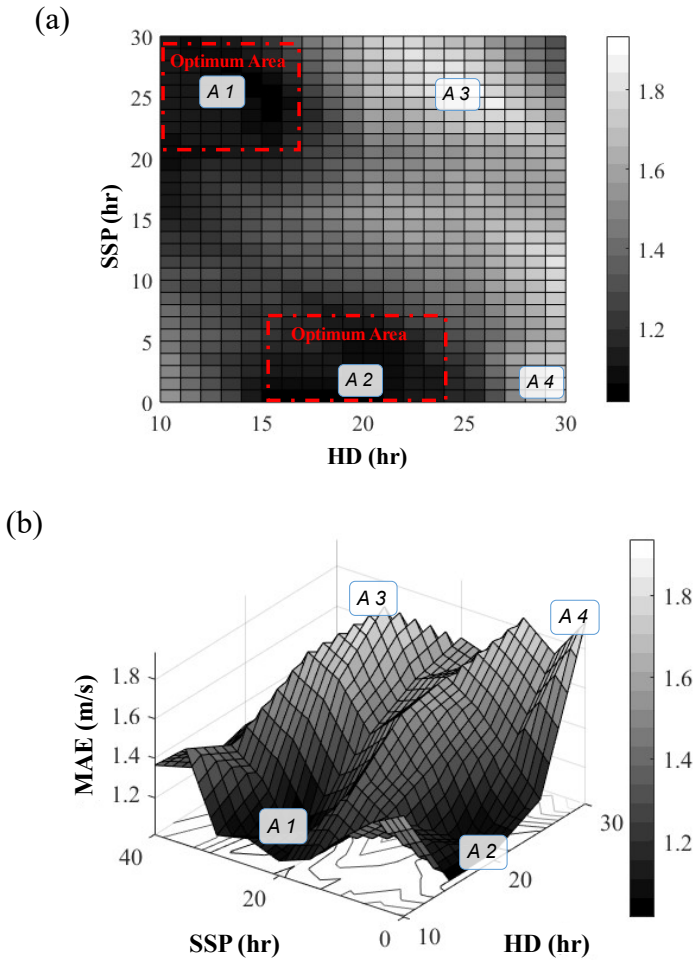

Figure 3-15. Grid search for finding optimal parameters: (a) 2D, (b) 3D.

Table 3-3 lists four models (labeled Models I, II, III, and IV) to compare the performances between models trained on different combinations of parameters. Figure 3-16 graphically shows the tuning results for each set of parameter settings. As this figure shows, the greater the number of parameters that were close to optimal areas, the higher was the prediction accuracy achieved by the tuned model with respect to not only MAE but also time delay between maximum points of actual and predicted wind speeds.

Table 3-3. Models and their design parameters

No.	Name	Design parameters			
		Category	Color	DH	SSP
1	Model I	A1 (Optimum)	Green	15	25
2	Model II	A2 (Optimum)	Yellow	20	00
3	Model III	A3	Cyan	20	15
4	Model IV	A4	Blue	25	25

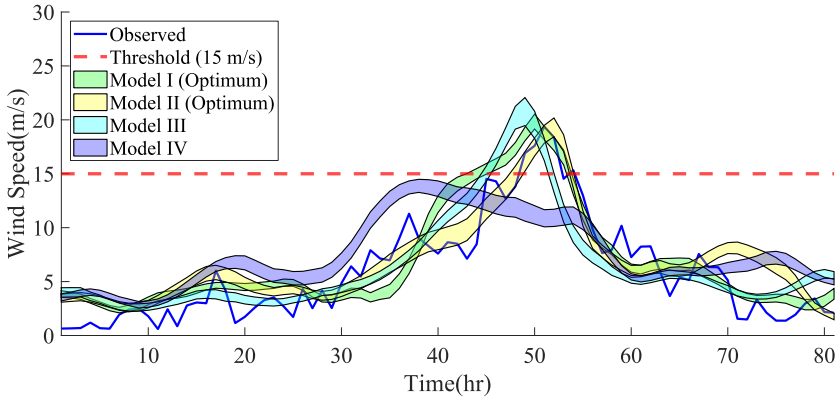

Figure 3-16. Tuning results for each set of parameter settings.

CHAPTER 4

DEVELOPMENTAL FRAMEWORK FOR OPERATIONAL INTELLIGENCE

This chapter provides an overview of the developmental frameworks and conducted validation studies for two long-span bridges to assess the framework applicabilities. Based on these results, their accuracies and feasibilities are comprehensively discussed in the second section of this chapter.

4.1 Developmental frameworks

This section introduces the two individual developmental frameworks for dealing with the two wind-induced problems. Schematic overviews are provided in Figure 4-1.

In the first framework, the primary part is a knowledge-based feature selection process, which is based on well-established wind engineering knowledge and observed vibration characteristics derived from SHM data. In the second part, an NN structure is designed with reference to the selected features. The third part is a training optimization process, consisting of soft labeling, supervised machine learning, and performance checks in terms of

the distributions of peak-factor and VA curves. In the final part, the performance of the trained model is applied to a long-span bridge.

In the second framework, the primary part is a knowledge-based feature selection process based on strong wind properties identified from well-established information about typhoons. In the second part, an NN structure is designed with reference to the selected features. The third part is the training optimization process that involves the selection of an influential typhoon, time-delay analysis, and a grid search-based tuning method. In the final part, the developed model is applied to a long-span bridge.

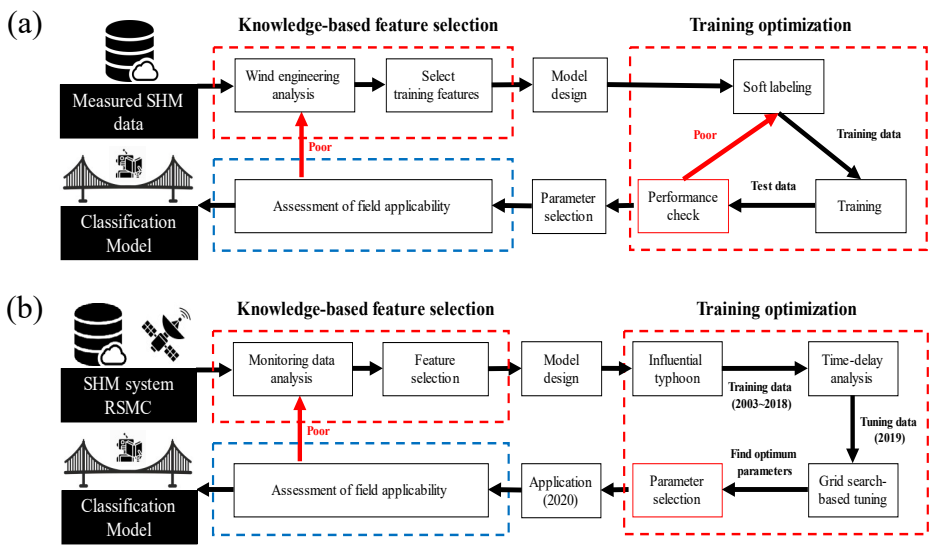

Figure 4-1. Developmental frameworks: (a) automated VIV classification, (b) short-term forecasting of typhoon-induced strong winds.

4.2 Assessment of field applicability

4.2.1 Data-driven automated VIV classification

This section presents a validation of the classification model trained on the optimal PFT-based datasets derived from the previous chapter. The PFT value was set to 1.7. The classification model was applied to long-term monitoring data collected from January to September 2019, the acceleration data for which included several types of vibrations such as fully or partially developed VIVs. Figure 4-2 verifies that the training process of the classification model was conducted appropriately.

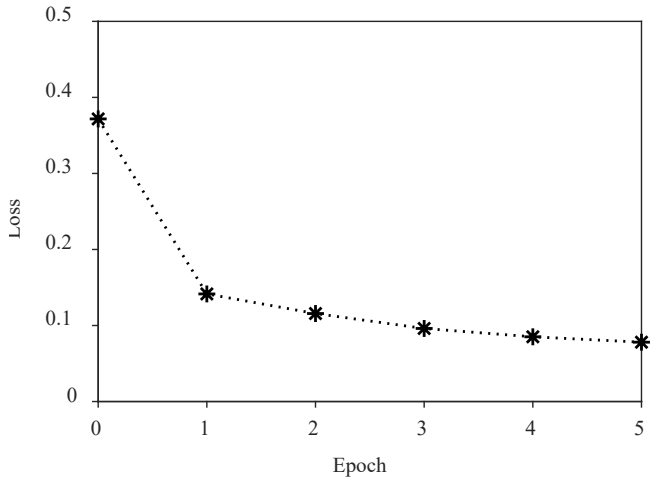

Figure 4-2. Loss value for each epoch.

The classification results were assessed using a VA curve and the corresponding confusion matrix, as shown in Figure 4-3. These results constituted 20% of the total available datasets. According to the basic assumption, a well-trained model should classify semi-VIVs as well as VIVs classified initially in the positive class. In our study, the number of FP cases was relatively high. However, the VA curve confirmed whether these FPs were actual false positive errors or should have been classified as semi-VIV. As expected, the FP and TP were located relatively close to each other, and most of their RMS acceleration values clearly showed the characteristics of VIV, indicating that the model extracted meaningful environmental conditions of VIV by reclassifying VIV cases (i.e., those not labeled initially as VIV) as VIV classes (FP).

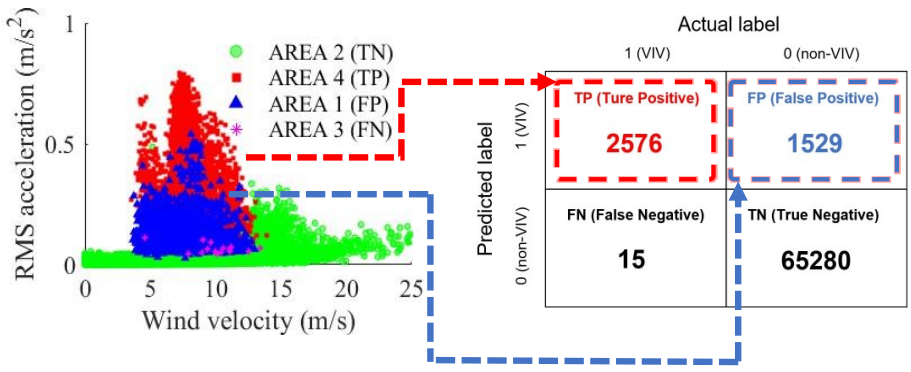

Figure 4-3. Classification results (PFT = 1.7).

Figure 4-4 shows representative examples of the four types of classification. As expected, FP included the semi-VIV cases, which could be considered as

cases of clear harmonic motion. The soft labeling used in this study ignored these cases because of the peak factor being higher than 1.7. However, the trained model classified this vibration as VIV. In addition, FN was completely negligible as compared to the total number of validation data, confirming that the trained model did not cause this type of error from an engineering point of view. Therefore, it could be confirmed that the training process through ANN sufficiently overcame errors during the labeling process and achieved more comprehensive classification results.

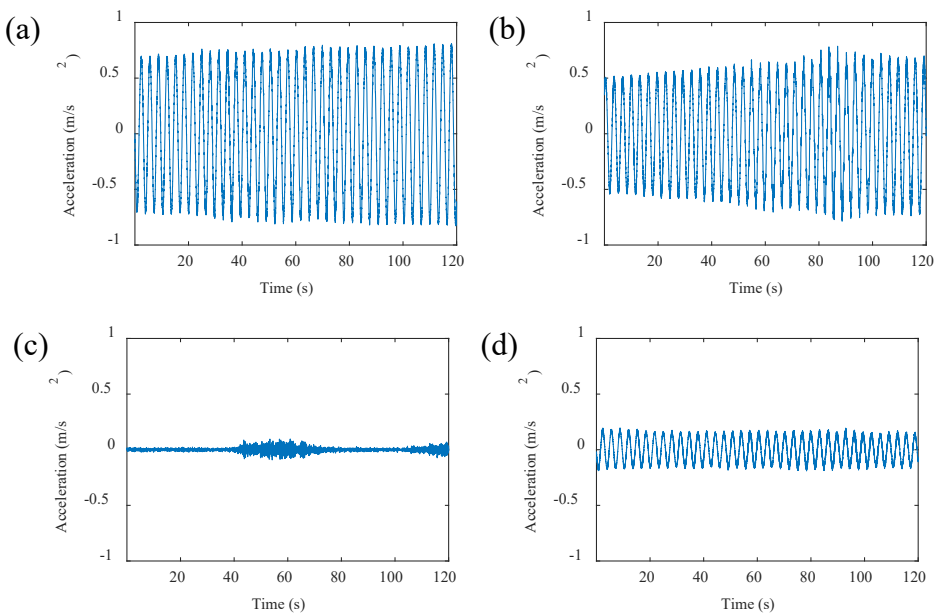

Figure 4-4. Time-history acceleration of the four areas: (a) TP, (b) FP, (c) TN, (d) FN.

4.2.2 Data-driven short-term forecasting of typhoon-induced strong winds

This section presents a validation of the developed prediction model. With the optimal parameters, the developed framework was applied in 2020 to two test typhoon events. One test event induced 1-h averaged strong surface wind speeds of over 15 m/s, which could be dangerous to vehicles traversing the bridge. Therefore, if the developed prediction model with optimal parameter settings was well trained, the time of occurrence of strong wind speeds for test typhoons could be predicted with accuracy. Figure 4-5 shows the time histories of selected features, routes, and satellite images for each test typhoon.

(a)

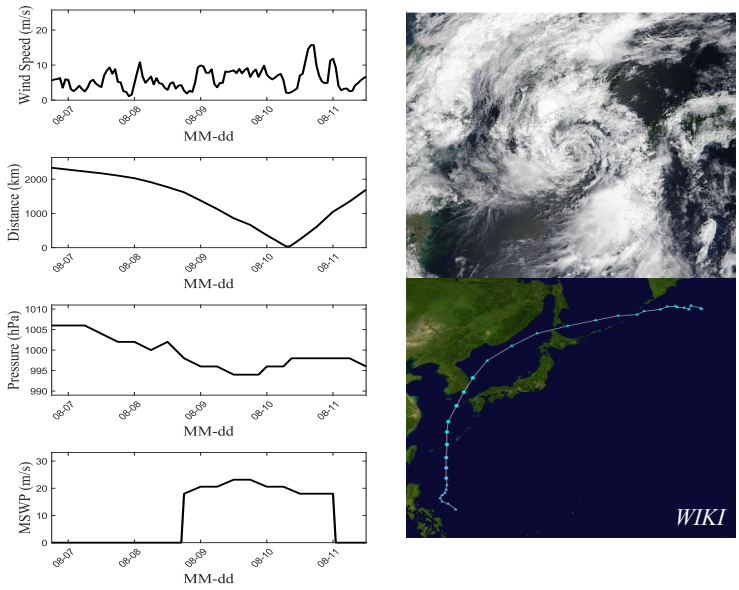

(b)

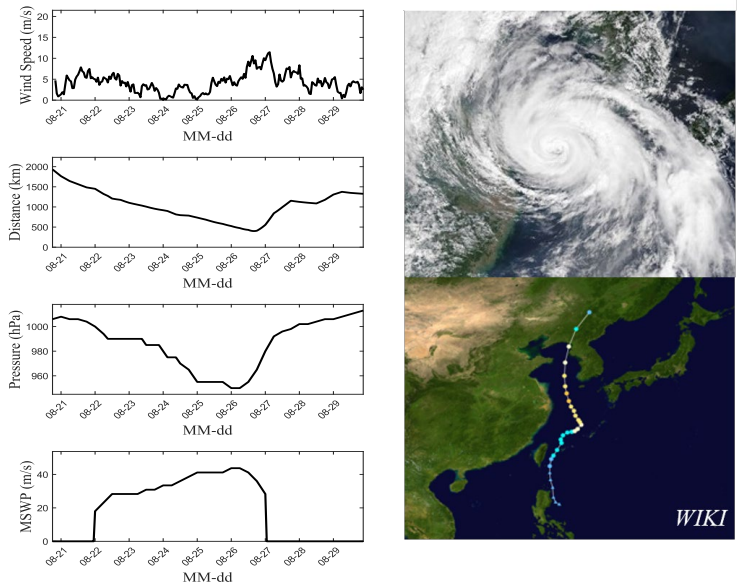

Figure 4-5. Test typhoons: (a) JANGMI (2020/08), (b) BAVI (2020/08).

Prediction results obtained from the developed models with an optimal combination of parameters are graphically shown in Figure 4-6. The x and y axes indicate relative time and 1-h averaged winds in the locations observed, respectively. Threshold (i.e.,15 m/s) and predicted wind speeds by the two models are plotted in blue, red, green, and yellow, respectively. If the forecasted wind speed was greater than the threshold value based on the predictions of the two optimal Models I and II, an early warning signal is automatically sent to the bridge operators.

First, with the green and yellow areas representing 95% CI analytical results, most of these areas show a narrow shape, which means that the prediction results were stable under intrinsic and extrinsic factors such as weight initialization or randomly partitioned datasets.

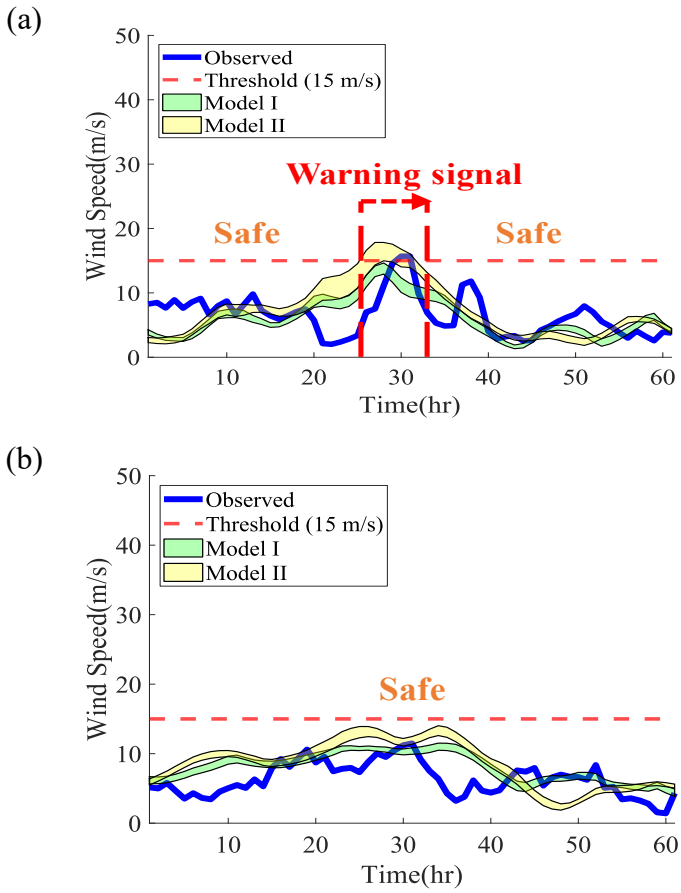

Figure 4-6. Prediction results: (a) JANGMI (2020/08), (b) BAVI (2020/08).

Second, all maximum wind speeds were well detected 6 h in advance, which was sufficient time for bridge operators to prepare for typhoon-induced strong winds. The prediction model could detect rising and falling trends, which are vital information for developing efficient traffic control systems. For example, if the control measure conducted on traffic lasts longer than necessary, this could cause substantial economic losses in logistics industries. However, if less than necessary, this could induce a hazard to vehicles traversing the bridge. Because the primary purpose of this study was to

determine whether traffic movement should be controlled, conducting this measure in a timely fashion was key to improving the control system reliability. Third, the developed model did not issue a warning message when a non-influential typhoon passed through the bridge, showing that the models well identified influential from non-influential typhoons during the year. This is important because a prediction model that issues warning signals regardless of the risk levels of each typhoon with respect to overturning vehicles could decrease the traffic control system's overall reliability. Finally, the developed models performed well with a simple structure and a relatively small amount of training data. Even though most of the long-span bridges we studied had a series of sensors, this does not ensure vast amounts of SHM big data. Considering that influential typhoons are highly likely to represent only a small portion of the total number of datasets, limits exist on the extent to which typhoon datasets can be used for the training process. From the perspective of bridge operators, developing a robust model to satisfy operator’s intentions despite the aforementioned shortcomings is desirable. Given this context, the proposed framework proved that, with relatively few observational datasets for 17 years from 2003 to 2019, typhoon-induced wind hazards were effectively detected. Therefore, it can be concluded that the framework can effectively support existing operating systems.

CHAPTER 5

CONCLUSION AND FURTHER STUDY

This research proposed general development frameworks for ML-based operational intelligence of long-span bridges to assist existing long-span bridge operational systems. The overall development frameworks for operational intelligence are illustrated in Figure 5-1.

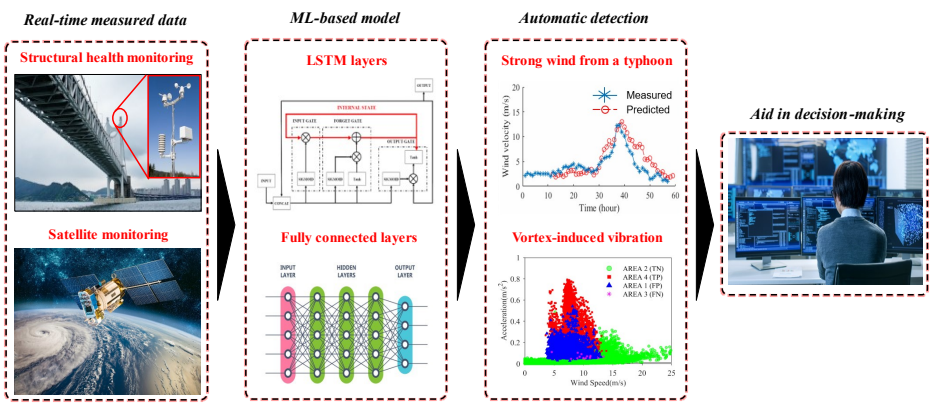

Figure 5-1. Development frameworks for operational intelligence.

First, two major wind-induced problems that occur on long-span bridges were defined, namely, VIVs and strong wind-induced accidents of overturning vehicles. Second, each model was developed with three main components: 1) knowledge-based feature selection, which considers optimal combinations of influential features, 2) ANN models to reflect the complex relationship between environmental or vibrational characteristics and the two wind-induced problems, and 3) parametric studies conducted for training

optimization to develop a customized model for each bridge. The developed frameworks were applied to the Gwangan and Cheonsa Bridges, both located in South Korea, to perform the validation process. Based on the results obtained from this study, the following conclusions can be drawn.

5.1 Conclusion

For VIV classification, the soft labeling method was demonstrated to be effective at detecting VIV within a certain PFT range. Numerical examples were given to demonstrate the feasibility of this approach by parametric sensitivity analysis. Even though the developed model underfitted the training data when PFT was set to less than 1.7, the positively classified distributions were skewed mainly toward the left, in contrast to the histograms of the natural peak factor. This result proved the robustness and feasibility of the proposed data-driven classification. By contrast, when PFT was set to greater than 2.0, the classification performance dramatically decreased because the training process intrinsically provided a greater number of opportunities to learn unrelated features from the training datasets. Therefore, the optimal PFT range could be considered to be in the range of 1.5 to 2.0.

The study showed that the proposed method provides a general data-driven framework to develop a VIV classification model for long-span bridges in operation. The selected features were shown to be simple, and training datasets could be effectively labeled using the soft-labeling method. More

importantly, the study showed that the suggested framework does not require any human-based threshold values of the selected environmental and vibrational features, which could be advantageous for existing bridge operating systems.

In terms of strong wind-speed forecasting, the four selected input features were: 1) distance between a typhoon and the bridge, 2) MSWS of a typhoon, 3) pressure of a typhoon, and 4) wind speed measured at the bridge. These were found to represent an appropriate combination. In addition, the adequacy of the training datasets significantly affected the performance of the developed model. It is recommended that care be taken in generating training datasets. The suggested framework well met the current needs of bridge operators with relatively few observational datasets for 17 years from 2003 to 2019 and proved that typhoon-induced wind hazards can be detected when using properly selected input features and suitable parameters.

5.2 Further study

The proposed frameworks provide useful tools for automatic VIV classification and strong wind-speed prediction during a typhoon. However, other research aspects must be studied. First, this work investigated a specific combination of influential features for use in designing and training the models. Considering the flexible nature of an NN, which can incorporate multiple influential features, the performance should be comprehensively studied with more diverse combinations of features. Second, this research selected only one bridge as a test-bed to assess the field applicability of each framework. More cases are recommended for examination to assess the general applicabilities of the frameworks. Therefore, applying the frameworks to a greater number of bridges is recommended for future studies.

REFERENCE

1. Abadi, M., et al. (2016). Tensorflow: A system for large-scale machine learning. 12th {USENIX} symposium on operating systems design and implementation ({OSDI} 16).

2. Abdalla, A. (2017). Advanced Wind Speed Prediction Model Based on a Combination of Weibull Distribution and an Artificial Neural Network. Energies, 10(11), 1744. doi:10.3390/en10111744

3. Al-Deen, S., Yamaguchi, A., Ishihara, T., & Bessa, R. (2006). A physical approach to wind speed prediction for wind energy forecasting. Journal of Wind Engineering, 349-352.

4. Al Jazeera English. (2018). Typhoon Jebi: Strongest storm to hit Japan in 25 years. Retrieved from https://www.youtube.com/watch?v =ZacWdCXQmCY

5. Alexiadis, M., Dokopoulos, P., Sahsamanoglou, H., & Manousaridis, I. (1998). Short-term forecasting of wind speed and related electrical power. Solar Energy, 63(1), 61-68.

6. Baker, C., & Reynolds, S. (1992). Wind-induced accidents of road vehicles. *Accident Analysis & Prevention, 24*(6), 559-575.

7. Bao, Y., Chen, Z., Wei, S., Xu, Y., Tang, Z., & Li, H. (2019). The state of the art of data science and engineering in structural health monitoring. Engineering, 5(2), 234-242.

8. Bearman, P. W. (1984). Vortex shedding from oscillating bluff bodies. AnRFM, 16, 195-222.

9. Blanchard, B. W., & Hsu, S. (2005). On the radial variation of the tangential wind speed outside the radius of maximum wind during hurricane Wilma (2005). Louisiana: Coastal Studies Institue, Louisiana State University, 1-11.

10. Cai, J., Luo, J., Wang, S., & Yang, S. (2018). Feature selection in machine learning: A new perspective. Neurocomputing, 300, 70-79.

11. Center, J. T. W. (2007). 3.3 JTWC Forecasting Philosophies. pdf). Retrieved, 11.

12. Chang, P.-C., Yang, R.-Y., & Lai, C.-M. (2015). Potential of Offshore Wind Energy and Extreme Wind Speed Forecasting on the West Coast of Taiwan. Energies, 8(3), 1685-1700. doi:10.3390/en8031685

13. Chih-Chiang, W., Po-Chun, P., Cheng-Han, T., & Chien-Lin, H. (2018). Regional Forecasting of Wind Speeds during Typhoon Landfall in Taiwan: A Case Study of Westward-Moving Typhoons. *Atmosphere, 9*(4), 141. doi:10.3390/atmos9040141

14. Damousis, I. G., Alexiadis, M. C., Theocharis, J. B., & Dokopoulos, P. S. (2004). A fuzzy model for wind speed prediction and power generation in wind parks using spatial correlation. IEEE Transactions on Energy Conversion, 19(2), 352-361.

15. De, S., Mukherjee, A., & Ullah, E. J. a. p. a. (2018). Convergence guarantees for RMSProp and ADAM in non-convex optimization and an empirical comparison to Nesterov acceleration.

16. Ding, N., Benoit, C., Foggia, G., Bésanger, Y., & Wurtz, F. (2015). Neural network-based model design for short-term load forecast in distribution systems. IEEE transactions on power systems, 31(1), 72-81.

17. Dupond, S. (2019). A thorough review on the current advance of neural network structures. Annual Reviews in Control, 14, 200-230.

18. Fairclough, H. E., Gilbert, M., Pichugin, A. V., Tyas, A., & Firth, I. (2018). Theoretically optimal forms for very long-span bridges under gravity loading. Proceedings of the Royal Society A: Mathematical, Physical and Engineering Sciences, 474(2217), 20170726.

19. Filik, T. (2016). Improved Spatio-Temporal Linear Models for Very Short-Term Wind Speed Forecasting. Energies, 9(3), 168. doi:10.3390/en9030168

20. Focken, U., Lange, M., Mönnich, K., Waldl, H.-P., Beyer, H. G., & Luig, A. (2002). Short-term prediction of the aggregated power output of wind farms—a statistical analysis of the reduction of the prediction error by spatial smoothing effects. Journal of Wind Engineering and Industrial Aerodynamics, 90(3), 231-246.

21. Gaarder, A. M. (2019). Aerodynamic wind analysis of bridge girder with CFD calculations. Norwegian University of Life Sciences, Ås,

22. Guoyang, W., Yang, X., & Shasha, W. (2005). Discussion about short-term forecast of wind speed on wind farm. Jilin Electric Power, 181(5), 21-24.

23. Han, J., Pei, J., & Kamber, M. (2011). Data mining: concepts and techniques: Elsevier.

24. Harper, B., Kepert, J., & Ginger, J. (2010). Guidelines for converting between various wind averaging periods in tropical cyclone conditions: WMO Geneva, Switzerland.

25. Hochreiter, S., & Schmidhuber, J. (1997). Long short-term memory. Neural Computation, 9(8), 1735-1780.

26. Huang, Z., et al. (2019). "Automatic Identification of Bridge Vortex-Induced Vibration Using Random Decrement Method." Applied Sciences 9(10): 2049.

27. Hwang, Y. C., Kim, S., & Kim, H.-K. (2020). Cause investigation of high-mode vortex-induced vibration in a long-span suspension bridge. Structure and Infrastructure Engineering, 16(1), 84-93.

28. Kim, S.-J., & Kim, H.-K. (2019). Feasibility of a Quasi-Static Approach in Assessing Side-Wind Hazards for Running Vehicles. *Applied Sciences, 9*(16), 3377.

29. Kim, S.-J., Shim, J.-H., & Kim, H.-K. (2020). How wind affects vehicles crossing a double-deck suspension bridge. Journal of Wind Engineering and Industrial Aerodynamics, 206, 104329.

30. Kim, S.-J., Yoo, C.-H., & Kim, H.-K. (2016). Vulnerability assessment for the hazards of crosswinds when vehicles cross a bridge deck. *Journal of Wind Engineering and Industrial Aerodynamics, 156*, 62-71.

31. Kim, S., Park, J., & Kim, H.-K. (2017). Damping identification and serviceability assessment of a cable-stayed bridge based on operational monitoring data. Journal of Bridge Engineering, 22(3), 04016123.

32. Kingma, D. P. and J. Ba (2014). "Adam: A method for stochastic optimization." arXiv preprint arXiv:1412.6980.

33. Ko, J., & Ni, Y. Q. J. E. s. (2005). Technology developments in structural health monitoring of large-scale bridges. 27(12), 1715-1725.

34. Kong, W., Dong, Z. Y., Jia, Y., Hill, D. J., Xu, Y., & Zhang, Y. (2017). Short-term residential load forecasting based on LSTM recurrent neural network. IEEE Transactions on Smart Grid, 10(1), 841-851.

35. Krogh, A. and J. A. Hertz (1992). A simple weight decay can improve generalization. Advances in neural information processing systems.

36. KSCE (2006). Design guidelines for steel cable bridges. Korean Society of Civil Engineers (in Korean)

37. Laima, S., Li, H., Chen, W., & Li, F. (2013). Investigation and control of vortex-induced vibration of twin box girders. Journal of Fluids and Structures, 39, 205-221.

38. Landsea, C. (2014). What regions around the globe have tropical cyclones and who is responsible for forecasting there. In: Hurricane Research Division, Atlantic Oceanographic & Meteorological ….

39. Lei, M., Shiyan, L., Chuanwen, J., Hongling, L., & Yan, Z. (2009). A review on the forecasting of wind speed and generated power. Renewable and Sustainable Energy Reviews, 13(4), 915-920. doi:10.1016/j.rser.2008.02.002

40. Li, G., & Shi, J. (2010). On comparing three artificial neural networks for wind speed forecasting. Applied Energy, 87(7), 2313-2320. doi:10.1016/j.apenergy.2009.12.013

41. Li, S., et al. (2017). "Cluster analysis of winds and wind-induced vibrations on a long-span bridge based on long-term field monitoring data." Engineering Structures 138: 245-259.

42. Lin, I., Wu, C.-C., Emanuel, K. A., Lee, I.-H., Wu, C.-R., & Pun, I.-F. (2005). The interaction of Supertyphoon Maemi (2003) with a warm ocean eddy. Monthly weather review, 133(9), 2635-2649.

43. Lumley, J. L., & Panofsky, H. A. (1964). The structure of atmospheric turbulence (Vol. 12): Interscience publishers New York.

44. Lv, Y., Duan, Y., Kang, W., Li, Z., & Wang, F.-Y. (2014). Traffic flow prediction with big data: a deep learning approach. IEEE Transactions on Intelligent Transportation Systems, 16(2), 865-873.

45. MacQueen, J. (1967). Some methods for classification and analysis of multivariate observations. Paper presented at the Proceedings of the fifth Berkeley symposium on mathematical statistics and probability.

46. Powell, M. D., Vickery, P. J., & Reinhold, T. A. (2003). Reduced drag coefficient for high wind speeds in tropical cyclones. nature, 422(6929), 279-283.

47. Sarpkaya, T. (2004). A critical review of the intrinsic nature of vortex-induced vibrations. Journal of Fluids and Structures, 19(4), 389-447.

48. Seo, J.-W., Kim, H.-K., Park, J., Kim, K.-T., & Kim, G.-N. (2013). Interference effect on vortex-induced vibration in a parallel twin cable-stayed bridge. Journal of Wind Engineering and Industrial Aerodynamics, 116, 7-20.

49. Srivastava, N., et al. (2014). "Dropout: a simple way to prevent neural networks from overfitting." The journal of machine learning research 15(1): 1929-1958.

50. Wang, Z., Wang, Y., & Srinivasan, R. S. (2018). A novel ensemble learning approach to support building energy use prediction. Energy & Buildings, 159, 109-122. doi:10.1016/j.enbuild.2017.10.085

51. Wei, C.-C. (2014). Surface Wind Nowcasting in the Penghu Islands Based on Classified Typhoon Tracks and the Effects of the Central Mountain Range of Taiwan. Weather and Forecasting, 29(6), 1425-1450. doi:10.1175/WAF-D-14-00027.

52. Wei, C. C. (2015). Forecasting surface wind speeds over offshore islands near Taiwan during tropical cyclones: Comparisons of data-driven algorithms and parametric wind representations. Journal of Geophysical Research: Atmospheres, 120(5), 1826-1847. doi:10.1002/2014JD022568

53. Williamson, C., & Govardhan, R. (2004). Vortex-induced vibrations. Annu. Rev. Fluid Mech., 36, 413-455.

54. Wu, W., May, R. J., Maier, H. R., & Dandy, G. C. (2013). A benchmarking approach for comparing data splitting methods for modeling water resources parameters using artificial neural networks. Water Resources Research, 49(11), 7598-7614.

55. Zhang, W., Wang, J., Wang, J., Zhao, Z., & Tian, M. (2013). Short-term wind speed forecasting based on a hybrid model. Applied Soft Computing Journal, 13(7), 3225-3233. doi:10.1016/j.asoc.2013.02.016

56. Zhu, L., Li, L., Xu, Y.-L., & Zhu, Q. (2012). Wind tunnel investigations of aerodynamic coefficients of road vehicles on bridge deck. *Journal of Fluids and Structures, 30*, 35-50.

APPENDIX

A. Influential typhoons

Table A.0-1 Influential typhoon list

No.	Name	Date	Route	Maximum wind-speed
1	LINFA	2003/05	East-Sea	16.1
2	SOUDELOR	2003/06	East-Sea	21.0
3	MINDULLE	2004/06	Inland	18.0
4	MEGI	2004/08	East-Sea	28.0
5	NABI	2005/08	East-Sea	24.7
6	SHANSHAN	2006/09	East-Sea	21.2
7	MANYI	2007/07	East-Sea	16.0
8	PABUK	2007/08	Inland	15.9
9	NARI	2007/09	Inland	19.7
10	MELOR	2009/09	East-Sea	15.1
11	DIANMU	2010/08	Inland	23.0
12	MERANTI	2010/09	Inland	16.4
13	MEARI	2011/06	Inland	15.0
14	MUIFA	2011/07	Inland	19.2
15	SANBA	2012/09	Inland	24.3
16	VONGFONG	2014/10	East-Sea	17.7
17	GONI	2015/08	East-Sea	20.5
18	CHABA	2016/09	East-Sea	28.5
19	PRAPIROON	2018/06	East-Sea	18.3
20	CIMARON	2018/08	East-Sea	20.9
21	SOULIK	2018/08	Inland	20.9
22	KONGREY	2018/09	Inland	31.5
23	DANAS	2019/07	Inland	18.7
24	RINGRING	2019/09	Inland	17.8
25	TAPAH	2019/09	East-Sea	24.4
26	MITAG	2019/09	Inland	19.3

국 문 초 록

임재영
건설환경공학부
서울대학교 대학원

본 연구는 장대교량에서 바람에 의해 발생할 수 있는 와류진동과 차량 전복사고를 모니터링 할 수 있는 머신러닝기반 지능운영전략 구축을 위한 프레임워크를 제시하였다. 이를 통해 현재 교량에서 발생하고 있는 와류진동을 자동으로 분류하고, 태풍에 의한 강풍발생 시간범위를 예측하여 신속하고 면밀한 제진 대책과 교통통제전략 수립에 기여하고자 하였다. 본 연구에서 구축된 두개의 프레임 워크는 실제 국내에서 운용되고 있는 장대교량에 적용하여 성능검토를 수행하였다.

데이터 기반 와류진동 자동분류 프레임워크는 기존의 풍공학적 지식을 토대로 와류진동 발생과 연관된 적절한 훈련특성들을 선정하고, 완전연결신경망을 도입하여 교량 거더의 진동 및 외부 환경조건들과 와류진동발현 사이의 다차원적인 관계의 효과적인 학습을 유도하였다. 본 연구에서는 교량마다 개별화된 모델을 구축할 수 있도록 하기 위하여 적절한 훈련데이터 생성을 위한 소프트라벨링 방법론을 제시하였다. 제안된 모델은 국내 장대교량에 적용하여 성능검토를 진행하였으며, 기계가 구조 건전성 모니터링 데이터를 기반으로 높은 정확도 수준에서 와류진동을 자동으로 학습하고 선별할 수 있음을 검증할 수 있었다.

데이터 기반 태풍에 의한 강풍예측 프레임워크는 기존의 풍공학적 지식을 토대로 강풍 발생과 연관된 적절한 훈련특성들을 선정하고, 시계열 학습이 가능한 장단기 메모리 신경망 모델을 도입하여, 태풍과 교량사이의 거리, 태풍의 압력, 중심최대풍속, 그리고 교량에서의 측정된 풍속과 강풍 발생시점 사이의 다차원적인 관계의 효과적인 학습을 유도하였다. 본 연구에서는 교량마다 개별화된 모델을 구축할 수 있도록 하기 위하여 태풍선별 기법과 적절한 훈련데이터 생성을 위한 그리드탐색 기반 파라메터 최적화기법을 제시하였다. 제안된 모델은 2020 년 한반도를 통과한 태풍들에 대해 성능검토를 진행하였으며, 유의미한 수준에서 강풍 발생시점을 예측할 수 있음을 검증할 수 있었다.

상기 검토결과를 근거로 본 연구에서 제시한 데이터기반 프레임워크들은 바람에 의해서 발생할 수 있는 두가지 문제들을 모니터링하기 위해서 유용하게 활용가능한 근거자료를 제공할 수 있을 것으로 기대되는 바이다.

주요어: 지능운영; 장대교량; 딥러닝; 구조건전성 모니터링

Student Number: 2019-21249